JOURNAL OF PETROLOGY | VOLUME 0 | NUMBER 0 | PAGES 1–28 | 2012 | doi:10.1093/petrology/egs073

Journal of Petrology Advance Access published November 3, 2012

Petrological Insights into Shifts in Eruptive Styles at Volcán Llaima (Chile)

C. BOUVET DE MAISONNEUVE[1]*, M. A. DUNGAN[1], O. BACHMANN[2] AND A. BURGISSER[3,4,5]

[1]UNIVERSITY OF GENEVA, EARTH AND ENVIRONMENTAL SCIENCES SECTION, 13 RUE DES MARAICHERS, 1205 GENEVA, SWITZERLAND

[2]INSTITUTE OF GEOCHEMISTRY AND PETROLOGY, DEPARTMENT OF EARTH SCIENCES, ETH ZURICH, CLAUSIUSSTRASSE 25, 8092 ZURICH

[3]CNRS/INSU, ISTO, UMR 7327, 45071 ORLÉANS, FRANCE

[4]UNIV. D'ORLÉANS, ISTO, UMR 7327, 45071 ORLÉANS, FRANCE

[5]BRGM, ISTO, UMR 7327, 45071 ORLÉANS, FRANCE

RECEIVED NOVEMBER 10, 2011; ACCEPTED SEPTEMBER 13, 2012

Tephra and lava pairs from two summit eruptions (AD 2008 and 1957) and a flank fissure eruption (~ AD 1850) are compared in terms of textures, phenocryst contents, and mineral zoning patterns to shed light on processes responsible for the shifts in eruption style during typical eruptive episodes at Volcán Llaima (Andean Southern Volcanic Zone, Chile). The mineralogy and whole-rock compositions of tephra and lavas are similar within eruptive episodes, suggesting a common magma reservoir for Strombolian paroxysms and lava effusion. The zoning profiles and textures of plagioclase record successive and discrete intrusions of volatile-rich mafic magma accompanied by mixing of these recharge magmas with the resident basaltic-andesitic crystal mushes that are commonly present at shallow levels in the Llaima system. Each recharge event destabilizes the plagioclase in equilibrium with the resident crystal mush melt and stabilizes relatively An-rich plagioclase, as is recorded by the numerous resorption zones. Lavas typically have ~15–20 vol. % more phenocrysts than the tephra. Differences in plagioclase and olivine textures and zoning, combined with different phenocryst contents, indicate that a greater volume fraction of recharge magma is present in the explosively erupted magma than in subsequent effusively erupted magma. We propose that Strombolian paroxysms at Volcán Llaima are triggered by interactions with large volume fractions of recharge magma, which decrease the bulk viscosity and increase the volatile contents of the erupted magmas, leading to the conditions required for the fragmentation of basaltic-andesite. Lava effusion ensues from reduced interactions with the recharge magma, after it has partially degassed and crystallized, thereby impeding rapid ascent. This process could be operating at other steady-state basaltic volcanoes, wherein shallow reservoirs are periodically refilled by fresh, volatile-rich magmas.

KEY WORDS: *eruption style; magma recharge; plagioclase textures; Strombolian; Volcán Llaima*

INTRODUCTION

Much progress has been made in the field of eruption forecasting with the development of increasingly precise geophysical monitoring tools (Neuberg, 2006; Sparks *et al.*, 2012). Records of seismic activity may be inverted to models of magma motion and rock failure at depth beneath active volcanic systems (e.g. Roman *et al.*, 2006; Sturton & Neuberg, 2006; Hammer & Neuberg, 2009). Three-dimensional seismic tomography has proven successful for the location of potential reservoirs containing a fraction of magmatic liquid, expressed as low-velocity zones (e.g. magma reservoir beneath Rabaul, Papua New Guinea; Finlayson *et al.*, 2003; Bai & Greenhalgh, 2005; beneath Mauna Loa and Kilauea, Hawaii; Okubo *et al.*, 1997). A centimeter-scale inflation or deflation of a volcanic system owing to the migration of magmatic fluids can be

*Corresponding author. Telephone: +41 (0) 22 379 66 60. Fax: +41 (0) 22 379 32 10. E-mail: caroline.bouvet@unige.ch

recorded by InSAR (e.g. Bathke *et al.*, 2011; Chadwick *et al.*, 2011), tilt-meter (e.g. Green *et al.*, 2006), or global positioning system (GPS) measurements (e.g. Jentzsch *et al.*, 2001; Lowry *et al.*, 2001; Geist *et al.*, 2006). This information contributes to better eruption forecasting.

However, predicting the style of an eruption remains a challenge of fundamental importance for risk assessment. The vast majority of active volcanoes display a range in eruption styles, from effusive lava flow or dome growth to the explosive output of pyroclasts by Strombolian, Vulcanian, or Plinian eruptions (depending on magma viscosity, gas content, magma volume, etc.). The interpretation of geophysical signals as predictors of eruption style will ultimately depend on a thorough understanding of the magmatic processes that operate during periods of volcanic unrest, and especially of the processes that control eruptive volume and vigor.

Many studies have addressed the mechanisms for a given eruption style to occur and the possible origin(s) of transitions in eruption style at mafic and silicic volcanic centers (e.g. McBirney & Murase, 1970; Blackburn *et al.*, 1976; Jaupart & Vergniolle, 1988; Alidibirov, 1994; Woods & Koyaguchi, 1994; Parfitt & Wilson, 1995; Woods, 1995; Dingwell, 1996; Gonnermann & Manga, 2003, 2007; Cashman, 2004; Houghton *et al.*, 2004; Polacci *et al.*, 2005; Mason *et al.*, 2006; Lautze & Houghton, 2007; Scandone *et al.*, 2007; Namiki & Manga, 2008; Pioli *et al.*, 2009; Kent *et al.*, 2010; Ruprecht & Bachmann, 2010; and references therein). However, a number of uncertainties remain and dynamics can change significantly between volcanic centers. The key parameters controlling eruption style are both intrinsic (magma density, viscosity, volatile-, phenocryst-, and microlite-content) and extrinsic (conduit geometry—width, shape, junctions, roughness) to the erupted magma. They ultimately define the mass discharge rate and the mechanism by which the erupted magma fragments. Extrinsic parameters are specific to a volcanic center, and require geophysical studies and/or long-term monitoring to be accurately defined. In addition, they are subject to rapid changes owing to conduit excavation or clogging after an eruptive episode. Intrinsic parameters, on the other hand, are more generic and similarities can be observed between volcanic centers. They are defined at depth within the reservoir, although they may evolve at shallower levels owing to magma degassing and crystallization during eruption. Defining the main parameters controlling the eruption style(s) of a given volcano is crucial for reliable eruption forecasting.

The application of petrology to volcanology-based questions may establish a link between surface-monitored signals and the subsurface processes that generate them (Blundy & Cashman, 2008). Magma chamber dynamics and recharge processes have been addressed in detail at a number of volcanic centers through the examination of phenocryst and microlite textures, compositions and mineral zoning (Streck *et al.*, 2002, 2005; Couch *et al.*, 2003*a*; Gioncada *et al.*, 2005; Browne *et al.*, 2006; Humphreys *et al.*, 2006). Because of the slow diffusion of the Si–Al pair, plagioclase is a particularly useful tracer of magmatic processes. It has a strong tendency to retain in its major-element zoning a record of associated magma compositions and crystallization conditions. Combining major element variations with trace element and/or isotopic compositions of plagioclase has proven to be a powerful tool for unraveling magma crystallization, assimilation, recharge, and mixing processes operating in magma reservoirs (Blundy & Shimizu, 1991; Singer *et al.*, 1995; Brophy *et al.*, 1996; Kuritani, 1998; Ginibre *et al.*, 2002; Landi *et al.*, 2004; Berlo *et al.*, 2007; Gagnevin *et al.*, 2007; Ginibre & Worner, 2007; Ruprecht & Worner, 2007; Andrews *et al.*, 2008). We combine information derived from whole-rock compositions and modal phenocryst populations with mineral compositions and zoning, with a particular emphasis on plagioclase textures and compositions, to explore parameters and processes that may explain the typical shifts from Strombolian paroxysms to lava effusion at Volcán Llaima (38·7°S, Chile).

This study is a petrological comparison of tephra–lava pairs produced during the AD 2008, 1957, and ~1850 eruptive episodes. The examination of plagioclase textures and co-variations in Fe concentration and An content allows the identification of texturally and compositionally distinct zones within plagioclase cores and rims, which can be attributed to specific processes such as crystallization in the shallow reservoir, crystallization in a deeper reservoir, resorption during multiple magma recharge events, and crystallization during ascent and eruption. The outermost zones of the phenocrysts, which reveal the latest history of the magma before eruption, suggest that, although lavas and tephra were produced by the same magma, they experienced different degrees of interaction with relatively mafic recharge magmas. Eruptive style appears to be partly controlled by the volume fraction of recharge magma present in an erupted body. The greater the fraction of recharge magma, the more explosive is that particular phase of activity. If this is a general relationship, the application of geophysical tools to the estimation of the volumes of resident and recharge magma could be useful for eruption forecasting at Volcán Llaima and other similar highly active volcanoes.

GEOLOGICAL SETTING AND STUDIED SAMPLES

Volcán Llaima is one of the most active volcanoes in Chile, with about one eruption every 6 years (Dzierma & Wehrmann, 2010) and a spacing between large eruptions of the order of 30–140 years (Naranjo & Moreno, 2005). It

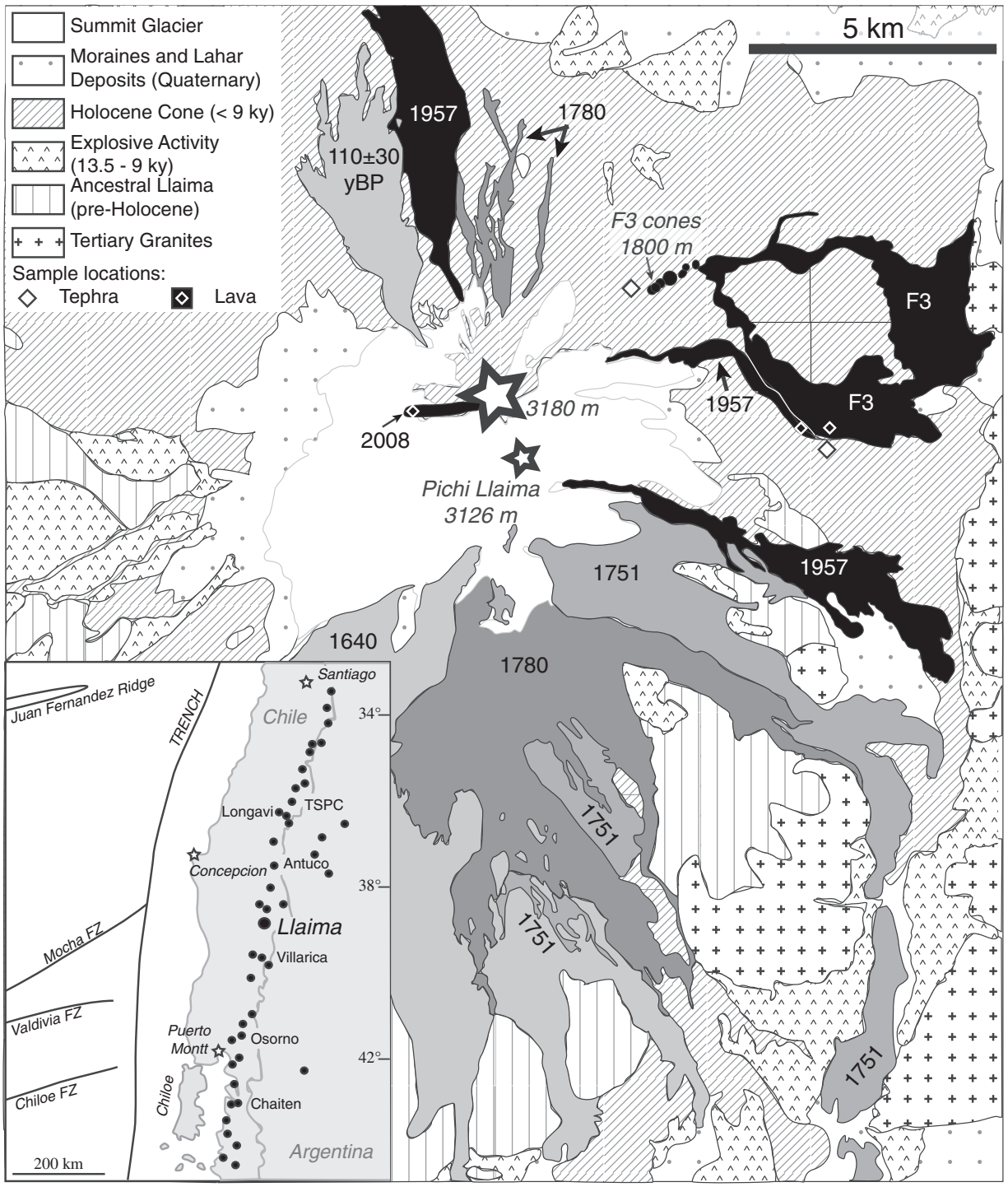

Fig. 1. Geological map of Volcán Llaima modified after Naranjo & Moreno (2005) and focused on the Holocene cone. Historical lava flows are labeled and prehistoric lava flows are undifferentiated and marked with oblique stripes. Two stars locate the summit vents; the larger one is the main crater and the smaller one is the 'Pichi Llaima' vent that was active during the 1957 eruptive episode. This study focuses on the 2008, 1957, and Fissural 3 (~ AD 1850) eruptive events. Tephra samples were taken from two stratigraphic sections, marked by black-outlined diamonds on the map. Lava samples were taken from the now eroded and buried January–February 2008 lava flow, the northeastern 1957 lava flow and the southern lobe of the Fissural 3 (F3, ~1850) lava flow. Sampling locations are marked with white diamonds. The inset in the lower left corner is a simplified map of the southern part of the Southern Volcanic Zone of the Andes. Volcán Llaima is located about 700 km south of Santiago.

undergoes very rapid resurfacing as a result of a combination of construction and erosion, dominantly by lahars, owing to its high eruption rate and the presence of extensive ice and snow cover at elevations >2500 m (Fig. 1). The youngest manifestations (~ AD 1850–2008) of the latest stage of cone-building activity at Volcán Llaima are numerous lava flows of basalt to basaltic-andesite associated with Strombolian activity. Eruptive episodes commonly last 1–3 years, including some short-term repose periods, and alternate between Strombolian paroxysms and effusion of mafic lavas (51–56 wt % SiO_2, 5–6 wt % MgO). The high frequency of eruptions and shifts in eruptive style make it an ideal place to investigate the processes at the origin of such shifts. Three relatively large eruptive episodes were selected and their tephra and lava products were compared to constrain the potential parameter(s) responsible for the shifts in eruption style.

The AD 2008, 1957, and ~1850 eruptive episodes

The 2008–2009 eruption is one of a few Llaima eruptions to have been sampled in real time. On January 1st, 2008, an ash plume rose from the central summit crater to an altitude of 12·5 km and drifted east and ESE (Smithsonian Institution, 2008). Emitted lava and incandescent material were initially confined to the crater, but within a few hours, a Strombolian phase began. Twelve hours of intense activity produced a thin, ~1 cm thick tephra layer on the lower eastern flank. Similar explosive (paroxysmal) events occurred subsequently in July 2008 and April 2009. Lava flows were extruded during January–February and July 2008, and then again during and after the early April 2009 paroxysm. The 2008 activity was trivial in volume and duration compared with the very large '1957' eruption, which also lasted 2 years. The thin, distal (3 km east of the summit) 2008 tephra deposit is now obscured by reworking and addition of the younger 2008 and 2009 tephra. The January–February 2008 lava was extensively eroded by lahars and then buried by the 2009 lava and is no longer accessible. Multiple comparably small eruptions of the late 20th century are no longer identifiable for similar reasons.

The '1957' eruption lasted 2 years and started in 1955. The general convention for protracted eruptions is to name the eruptive episode by the year it began. However, to be coherent with the geological map (Naranjo & Moreno, 2005) and a previous paper on Volcán Llaima (Bouvet de Maisonneuve *et al.*, 2012), we refer to the 1955–1957 eruptive episode as the 1957 event. This event produced three voluminous lava flows on the northern, northeastern, and eastern flanks of the volcano (Fig. 1). The northern flows were produced by the main central summit vent, whereas the eastern flow originated from 'Pichi Llaima', a summit vent slightly to the south of the main crater. Little is known about the temporal evolution of the eruption. The ~10 cm thick tephra unit linked to this eruption is preserved on the east flank, in accord with the prevailing wind direction. It must correspond to a voluminous paroxysm, as it is about 10 times thicker than the 2008 tephra, which has a very similar geographical distribution and was produced by a vigorous Strombolian eruption that lasted ~12 h.

The youngest pyroclastic and lava products from the system of lower flank fissures on Llaima were referred to by Naranjo & Moreno (2005) as the Fissural 3 episode (Fig. 1). This activity was inferred to have been prehistoric, but the stratigraphic position of the tephra close to the 1957 tephra deposit, the youthful appearance of these units, and a new ^{14}C date encourage us to place this activity at ~ AD 1850. The Fissural 3 eruption occurred from two parallel chains of cones on the northeastern flank of the volcano. Related tephra directly underlie the 1957 tephra layer. Two locally thick tephra layers (described as lower and upper or LF3 and UF3; ~15 cm thick) have been traced back to the two sets of cones, and must correspond to a paroxysmal eruption similar in volume or greater than the 1957 event. Voluminous lava flows are associated with the younger set of cones, and these are covered with tephra from the same eruption.

Studied tephra and lava samples

Tephra samples were collected from the January 1st, 2008 paroxysm, the 1955–1957 tephra bed, and the upper ~1850 tephra deposit (UF3) that is associated with the ~1850 lava flow (F3). Mafic scoria 2–5 cm in diameter were collected from two proximal stratigraphic sections located to the NE of the volcano in the direction of prevailing winds (Fig. 1; same samples as used by Bouvet de Maisonneuve *et al.*, 2012). The studied lava samples were selected from a large sample suite (~30 samples) and correspond to the January–February 2008 lava flow, the northeastern '1957' lava flow, and the south lobe of the ~1850 lava flow (Fig. 1). The other 1955–1957 lavas are compositionally and texturally very similar to the northeastern lava, and olivine populations from multiple flows are closely comparable. Some historical Llaima eruptive products are compositionally heterogeneous, but the 1957 products are among the most homogeneous (Dungan *et al.*, 2009).

All three eruptive events produced tephra and lavas of basaltic-andesitic composition (51–55 wt % SiO_2, 5–6 wt % MgO). The erupted products contain large crystals of plagioclase and olivine (Fig. 2). Small, light green pyroxenes occur in rare swarms in the Fissural 3 lava only, and oxides are either disseminated in the matrix or occur as very rare inclusions in the phenocrysts. Crystals are sub-millimeter to millimeter sized in the tephra, and the matrices are glassy with small disseminated plagioclase microlites. Crystals in the lavas span a range in size from microlites to millimeter sized crystals. The matrices are holocrystalline with olivine and plagioclase microlites. Weak preferred

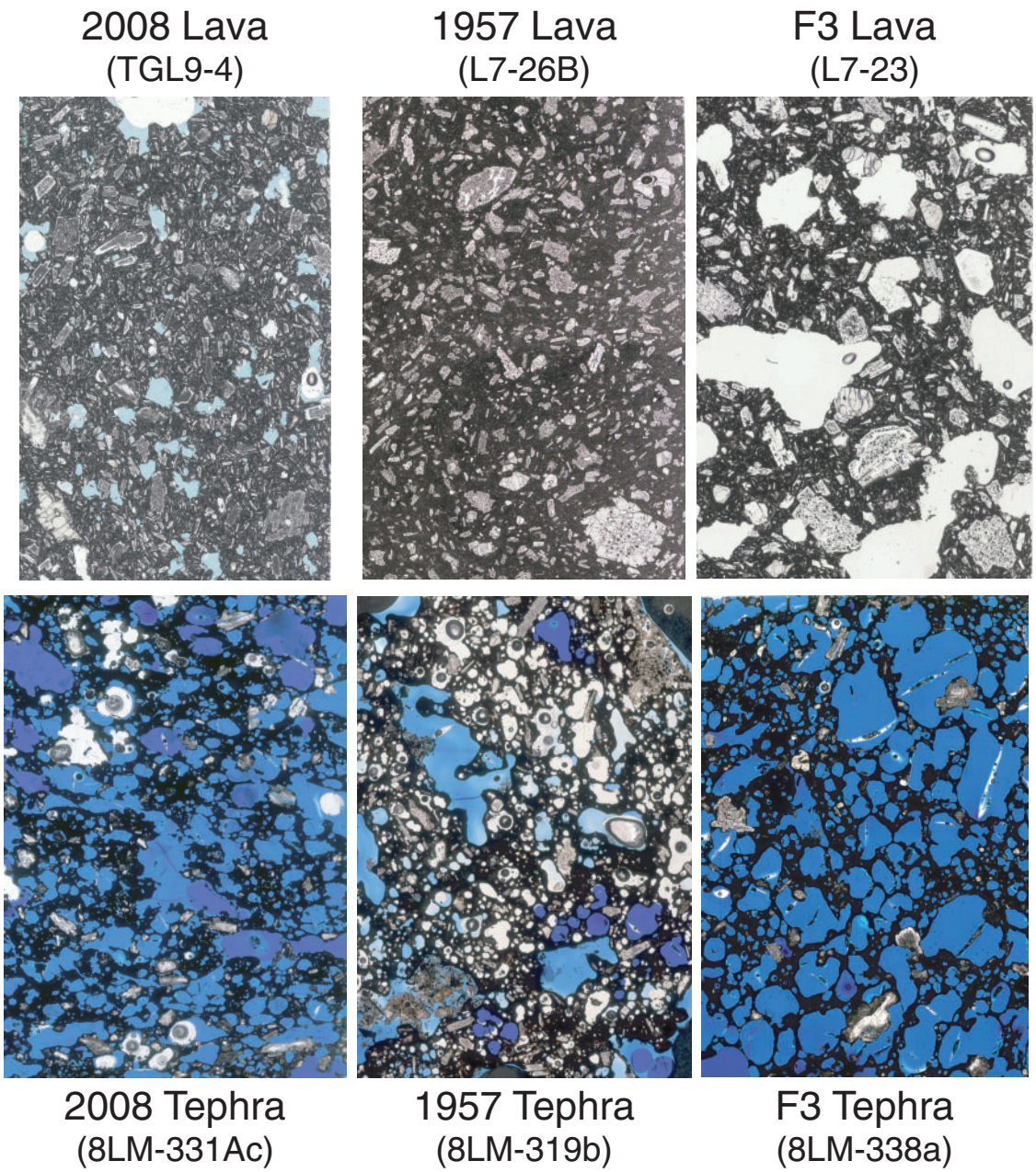

Fig. 2. High-resolution thin-section scans (~1 cm × 1·5 cm) showing higher crystallinities and lower vesicularities for the lavas (top) than the tephra (bottom). Phenocrysts are similar in size, and plagioclase crystals are frequently strongly resorbed. Epoxy was dyed blue in some cases to highlight the vesicles.

crystal orientations are locally developed, although crystals are more frequently randomly distributed.

Olivine and plagioclase phenocrysts are generally euhedral to subhedral and frequently occur as aggregates. Although the largest olivines are rounded and some display large embayments, the main deviation from euhedral shapes is due to crystals aggregating with each other and merging into one grain with a complex shape. The vast majority of plagioclase crystals contain melt inclusions, although some melt inclusion-free phenocrysts were observed in the lavas, but not in tephra. Melt inclusions may be concentrated in cores, near rims, in concentric zones, or be present throughout entire crystals. They are often glassy and contain vapor bubbles in the tephra, but are frequently recrystallized in lavas. The average volume fraction of crystals greater than 40 μm in diameter was estimated by point counting on scanned thin sections, and computed on a vesicle-free basis to ~23 vol. %, ~20 vol. %,

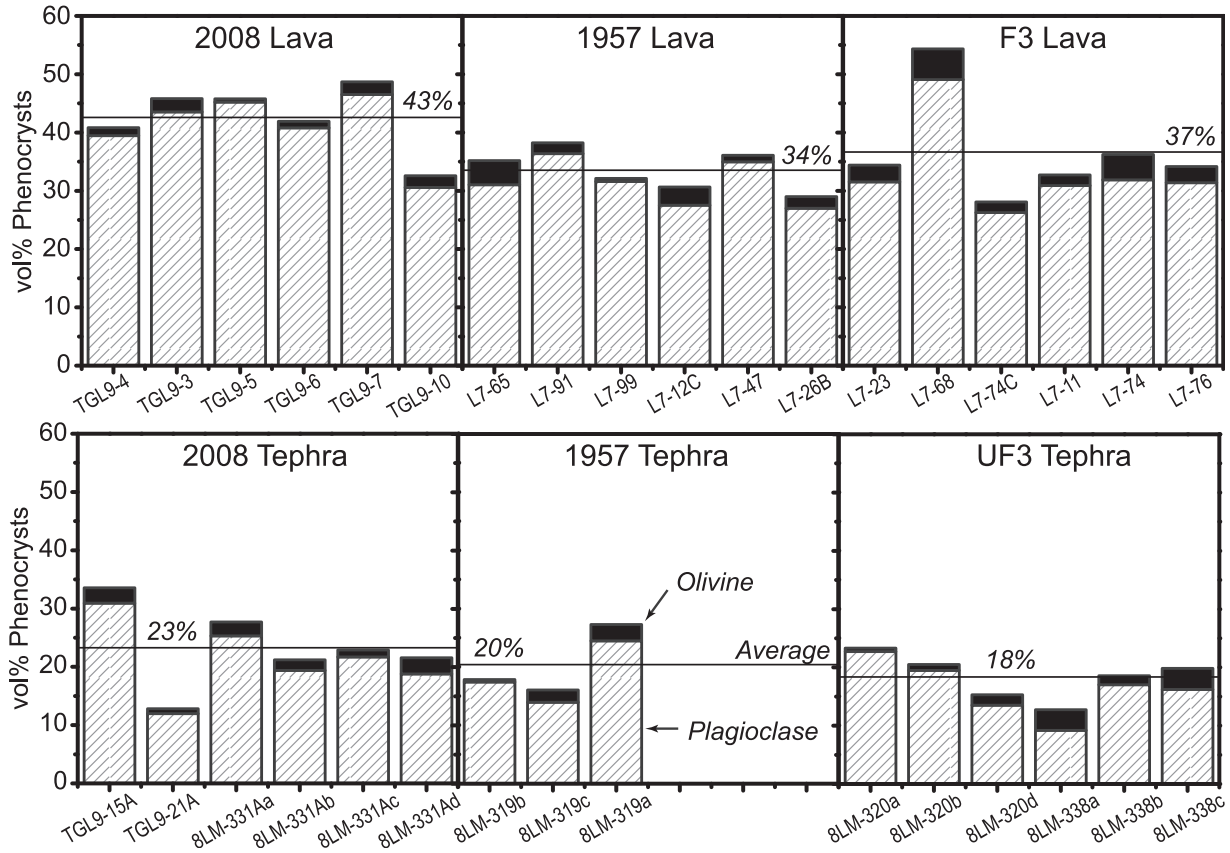

Fig. 3. Phenocryst contents of lavas and tephra estimated by point counting and computed on a vesicle-free basis on six thin sections per unit (except for the 1957 tephra, which were too small to make multiple thin sections). High-resolution thin-section scans were analyzed using the image analysis software JMicroVision (Roduit, 2002). A total of 400 points were considered per thin section, but evolution plots suggest that the phase proportions are correctly determined after ~150–200 points. The smallest identifiable crystals were at least ~40 μm in diameter. These set the threshold between phenocrysts and microlites. Plagioclase and olivine are in proportions 9:1 in both lavas and tephra. Lavas, however, contain about 15–20 vol. % more phenocrysts than in the associated tephra.

and ~18 vol. % for the 2008, 1957 and UF3 tephra deposits respectively, and ~43 vol. %, ~34 vol. %, and ~37 vol. % for the 2008, 1957 and Fissural 3 lava flows respectively (Fig. 3).

ANALYTICAL METHODS AND TERMINOLOGY

Whole-rock major and trace element compositions of tephra and associated lava flows were obtained by X-ray fluorescence (XRF) at the University of Lausanne (UNIL; Switzerland) and have been reported previously by Bouvet de Maisonneuve *et al.* (2012). Olivine crystals were analyzed by electron microprobe from three thin sections per unit for the lavas and one grain mount per unit for the tephra (Bouvet de Maisonneuve *et al.*, 2012). Olivines from the tephra are biased toward larger grain sizes owing to the fact that they were hand-picked to make the grain mounts. Extensive overlap of the tephra and lava data suggests that this bias did not affect the results. Plagioclase crystals were analyzed from one thin section per unit for the lava and tephra.

Major and minor element analyses by electron microprobe (JEOL 8200 electron microprobe at UNIL) were performed on ~100 olivine and 57 plagioclase crystals from the tephra, and ~100 olivine and 70 plagioclase crystals from the lava. Olivines were analyzed at 40 nA with a focused beam. Four to six point zoning profiles were obtained for the crystals from tephra and detailed traverses (5–20 μm point spacing) were obtained for those from the lavas. Counting time was 10/5 s (peak/background) for Si and Al, 30/15 s for Ca, and 20/10 s for the other elements. Plagioclase crystals were analyzed with a 5 μm diameter beam and 10 nA current. K and Na were analyzed first. Counting time was 10/7 s (peak/background) for Na, 10/5 s for K, 20/10 s for Si, Ca, and Al, and 50/25 s for Sr and Fe. A second series of analyses was conducted for a wider range of minor elements with longer counting times: 240/120 s for Sr, Fe, Mg, and Ti. Mineral standards were used and the relative error on major elements is around 1% for

SiO_2 and MgO, 2% for FeO, and 30% for MnO in olivine, and around 2% for SiO_2 and Al_2O_3, 3% for CaO, and 20% for Na_2O in plagioclase. Mineral chemical data are presented as Supplementary Data (available for downloading at http://petrology.oxfordjournals.org/).

The term phenocryst will be used frequently hereafter. However, it is ambiguous, as it can have a textural (i.e. a large crystal in a finer matrix) or genetic (i.e. referring to the pulse of magma from which it crystallized) connotation. W. Hildreth was the first to propose the term antecryst (presentation at Penrose Conference on 'Longevity and Dynamics of Rhyolitic Magma Systems', 2001) to distinguish crystals that have grown from a common but potentially complex magmatic system with a prolonged history, from crystals that grew exclusively from a distinct pulse or increment of magma in a spatial and temporal sense. Crystals that were incorporated from the surrounding host-rocks during transit and emplacement are usually termed xenocrysts. Following this definition, researchers have attempted to fully describe and classify crystal populations as phenocrysts (or autocrysts), antecrysts, and xenocrysts (Bacon & Lowenstern, 2005; Charlier *et al.*, 2005; Miller *et al.*, 2007; and references therein). In this study, we use the term phenocryst with a textural connotation only, and arbitrarily set the limit between phenocrysts and microlites at ~40 μm based on the image resolution of scanned thin sections. The validity of such a choice is discussed below in the section 'Timing and location of crystallization'. In terms of origin, the Llaima phenocrysts are dominantly antecrysts, which crystallized from earlier pulses of magma and were then incorporated in later pulses as discussed below. The smaller phenocrysts (down to 40 μm) probably have much shorter and simpler histories.

PETROGENESIS

The dynamics of magma storage, crystallization and recharge at Volcán Llaima have been addressed by Bouvet de Maisonneuve *et al.* (2012) in a combined study of olivine-hosted melt inclusions and zoning profiles of the host olivines from the same tephra units as studied here (2008, 1957 and Fissural 3 eruptions). The study revealed the presence of evolved basaltic-andesitic liquids (56 wt % SiO_2) trapped in olivine phenocrysts of variable compositions, and supports a model in which magmas are stored in a highly crystalline state (~55–60 vol. % crystals) in shallow dike-like reservoirs. These evolved liquid compositions are not observed in the whole-rock compositional range and are inferred to represent interstitial melts produced during the formation of a crystalline mush. Low H_2O–CO_2-saturation pressures (≤100 MPa) obtained from volatile contents in the olivine-hosted melt inclusions imply shallow magma storage less than ~4 km below the base of the edifice. The wide range in olivine core compositions and the absence of correlated H_2O–CO_2 degassing and magma evolution trends are interpreted to be due to magmas separately crystallizing, differentiating, and degassing in multiple, vertically extended reservoirs. Eruption triggering by the injection of mafic magma into these shallow reservoirs is supported by a preponderance of reversely zoned olivines in tephra.

The liquid line of descent represented by the compositional range of the entire volcano corresponds to a tholeiitic differentiation trend, as shown by the early enrichment in Fe and Ti (Fig. 4). It can be approximated with the thermodynamic algorithm MELTS (Ghiorso & Sack, 1995; Asimow & Ghiorso, 1998) considering a low pressure of 100 MPa, low volatile contents of the order of 1 wt % H_2O and 150 ppm CO_2, and an oxygen fugacity between the nickel–nickel oxide (NNO) and quartz–fayalite–magnetite (QFM) buffers. This is in agreement with the observations of Bouvet de Maisonneuve *et al.* (2012), except for the lower H_2O contents than measured in the olivine-hosted melt inclusions (2–3 wt %). The starting composition is an olivine-hosted melt inclusion from the UF3 tephra layer (~ AD 1850), for which the major element composition is reported in Table 1. A difficulty in reproducing the melt inclusion trend is the tendency of the thermodynamic model to overestimate the stability of clinopyroxene, as reported by Gaetani *et al.* (1998) and Villiger *et al.* (2007). High TiO_2 and low Al_2O_3 recorded by the evolved melt inclusions could be reproduced only when crystallization of this phase was artificially impeded. The close reproductions of melt inclusion and whole-rock trends, mineral phases, and mineral compositions requires a combination of equilibrium and fractional crystallization, a variation in oxygen fugacity from QFM to NNO, and the variable presence of pyroxene (Table 2 and Fig. 4). The necessity for a range in parameters (albeit limited) to explain crystallization trends at Llaima is consistent with the general model of multiple reservoirs that occasionally interact.

The overall successful reproduction of the compositional variation observed at Volcán Llaima considering a single parent magma and a low pressure of 100 MPa implies that the compositional variation of whole-rocks and melts is due to crystallization processes. It also suggests that (1) the composition of the parent or recharge magma did not change significantly with time, and (2) crystallization essentially takes place at low pressures. The crystal contents of the resident mush bodies can be approximated by the maximum amount of crystallization required to reproduce the olivine-hosted melt inclusion trend, and corresponds to ~55–60 vol. % crystals (Fig. 4). On the other hand, the parent magma composition can be approximated by a liquid composition (olivine-hosted melt inclusion), suggesting that it is close to aphyric. This is consistent with a mafic, low-viscosity magma travelling to shallower depths and losing its crystals on its way owing to gravitational

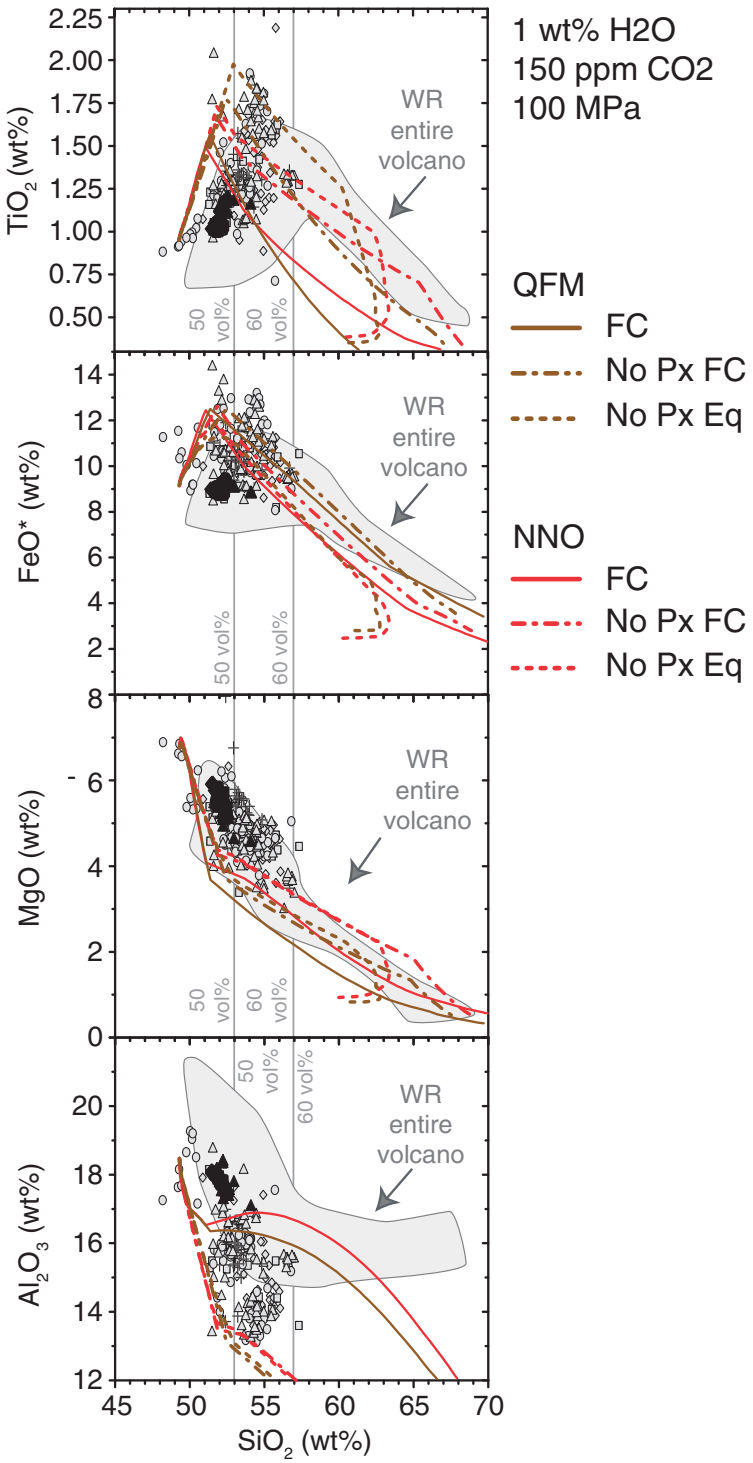

Fig. 4. Thermodynamic modeling of melt inclusion and whole-rock compositional trends using MELTS (Ghiorso & Sack, 1995; Asimow & Ghiorso, 1998). Shaded areas are the whole-rock trend of the entire volcano; black symbols represent the whole-rock compositions of the 2008 (diamonds), 1957 (squares), and Fissural 3 (triangles) eruptive events; crosses represent matrix glass compositions; gray symbols correspond to olivine-hosted melt inclusions from the 2008 (diamonds), 1957 (squares), upper (circles) and lower (triangles) Fissural 3 tephra units described by Bouvet de Maisonneuve *et al.* (2012). Continuous and dashed lines correspond to the evolution of the liquid composition as the result of isobaric cooling considering a constant pressure of 100 MPa and the initial presence of 1 wt % H_2O and 150 ppm CO_2 in the parent magma, which is in general agreement with the melt inclusion data (Bouvet de Maisonneuve *et al.*, 2012). The starting composition is an olivine-hosted melt inclusion from the UF3 tephra layer (Table 1). A small range in oxygen fugacity and crystallization type is required to reproduce the entire melt inclusion trend. Red lines are at NNO; brown lines are at QFM, and best reproduce the high TiO_2 contents reported by the melt inclusions. Dashed lines were obtained when the crystallization of pyroxene was artificially impeded, and best reproduce the low Al_2O_3 contents reported by the melt inclusions. Both fractional and equilibrium crystallization were considered (dash–dot and dashed lines respectively), but do not seem to yield much difference. Melt and whole-rock compositional trends generally overlap, but diverge for Al_2O_3 owing to the voluminous amount of plagioclase crystallization.

Table 1: Major element composition of the olivine-hosted melt inclusion from UF3 considered as a starting composition for geochemical modeling with MELTS

SiO_2	TiO_2	Al_2O_3	FeO*	MnO	MgO	CaO	Na_2O	K_2O
49·86	0·96	18·69	8·56	0·17	6·84	10·75	2·90	0·46

Table 2: Mineral phases crystallized by MELTS

	Pl	Ol	Sp	Cpx	Opx	Hbl	Bt	Sph	H_2O
QFM–FC									
Comp	$An_{83–23}$	$Fo_{81–60}$	x	x					x
App	0–85	4–63	49–85	20–85					76–85
@ 50	55·7	14·1	5·6	24·6					0
@ 60	57·2	13·2	6·7	23·0					0
QFM–FC–NoPx									
Comp	$An_{83–56}$	$Fo_{81–51}$	x			x		x	
App	0–75	4–71	48–75			71–75		74–75	
@ 50	70·7	24·5	4·8			0		0	
@ 60	69·8	23·9	6·3			0		0	
QFM–Eq–NoPx									
Comp	$An_{83–57}$	$Fo_{81–52}$	x			x		x	x
App	0–99	4–99	53–99			81–99		70–88	81–99
@ 50	73·2	26·3	0·5			0		0	0
@ 60	72·2	26·4	1·4			0		0	0
NNO–FC									
Comp	$An_{84–24}$	$Fo_{83–72}$	x	x	x				x
App	0–84	6–57	49–84	16–76	59–84				77–84
@ 50	53·5	10·8	8·2	26·1	1·5				0
@ 60	54·2	9·9	8·7	24·7	2·5				0
NNO–FC–NoPx									
Comp	$An_{84–54}$	$Fo_{83–66}$	x			x		x	
App	0–75	6–69	46–75			70–75		70–75	
@ 50	70·5	22·4	7·0			0		0	
@ 60	69·7	22·0	8·3			0		0	
NNO–Eq–NoPx									
Comp	$An_{84–57}$	$Fo_{83–57}$	x			x	x	x	x
App	0–99	6–99	48–99			75–99	95–99	99	85–99
@ 50	73·9	23·7	2·5			0	0	0	0
@ 60	72·8	23·6	3·6			0	0	0	0

FC, fractional crystallization; Eq, equilibrium crystallization; NoPx, pyroxene crystallization was artificially impeded; Comp, composition of the phase (x marks the presence of a phase); App, appearance of the phase in terms of wt % crystallization of the liquid; @ 50, wt % of the phase at 50 wt % crystallization of the liquid; @ 60, wt % of the phase at 60 wt % crystallization of the liquid.

settling. We infer from this that two end-member magmas interact during a recharge event; one is the highly crystalline resident mush that was formed by degassing and crystallization at shallow depths and the second is the parent magma that frequently replenishes the shallow magma reservoir. Low FeO and TiO_2 contents in the 53–60 wt % SiO_2 range that are not reproduced by the thermodynamic model are most probably the result of such mixing (Fig. 4).

To summarize, the dynamics of magma storage, crystallization and recharge at Volcán Llaima consists of a balance between (1) frequent replenishment of shallow magma reservoirs by the injection of mafic, crystal-poor magma, (2) intense crystallization following decompression and degassing of the recharge magma, and (3) frequent eruption of crystal-rich basaltic-andesitic magma. Bearing this specific geological setting in mind, tephra and lava samples were studied in detail to identify processes that occur just prior to or during an eruption and can explain the shifts in eruption style from Strombolian explosions to lava effusion. Information on such processes is potentially preserved in the details of the mineral textures, compositions and zoning. The following sections aim at identifying which crystals or parts of crystals were formed when and where, and what their implications are in terms of eruption dynamics.

MINERAL ZONING

Olivine

Low-resolution (~50 μm point spacing) zoning traverses across olivine crystals from the tephra record diverse core compositions and zoning trends in each sample, as discussed by Bouvet de Maisonneuve *et al.* (2012). Cores range from Fo_{67} to Fo_{84}, impeding the identification of 'equilibrium' populations (Fig. 5). Rim compositions in the three studied tephra units span a slightly narrower range ($Fo_{75–81}$) that is focused around $Fo_{78–80}$. Zoning profiles record non-zoned, normally zoned, and reversely zoned olivines, but reversely zoned olivines are the most common.

Detailed zoning profiles across olivine crystals from lavas show the same ranges in olivine core compositions as do those in associated tephra deposits ($Fo_{67–84}$; Figs 5 and 6), but zoning profiles in lavas are often slightly more complex, with reversely zoned shoulders adjacent to normally zoned rims (e.g. 2008 and 1957 samples). Rims are commonly characterized by sharp decreases in Fo content down to Fo_{65} or less within the outer 40 μm, especially in samples from 1957 and Fissural 3. When present, reversely zoned shoulders span the same compositional ranges as do olivine rims from the corresponding tephra ($Fo_{75–81}$; Fig. 6). Olivine zoning profiles in Fissural 3 lava samples are simpler, with few reversely zoned shoulders but a range in both core and rim compositions.

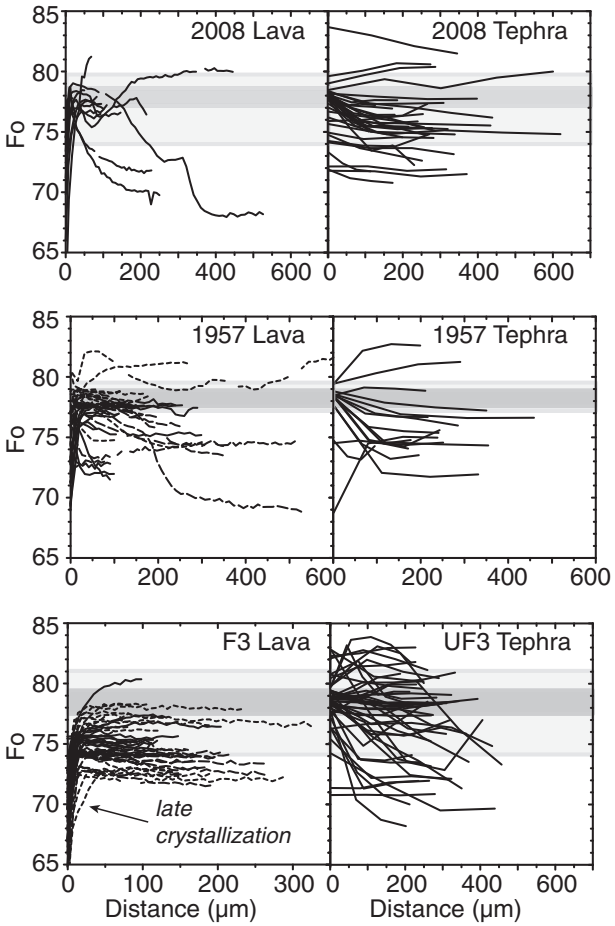

Fig. 5. Core–rim zoning profiles of olivines from the lava (left) and tephra (right) showing a similarly large range in core compositions. Crystals in tephra are dominantly reversely zoned and rim compositions focus around the same Fo contents. Crystals in lavas show more complex zoning at the rim with reversely zoned shoulders before a normally zoned rim. Where present, reversely zoned shoulders tend to focus around the same Fo contents as the olivine rims from the tephra. Crystals without reversely zoned shoulders are normally zoned with rim compositions that do not converge (e.g. Fissural 3 lava).

Plagioclase textures

Plagioclase phenocrysts are texturally extremely variable as shown on back-scattered electron (BSE) images (Fig. 7). The vast majority of these are extensively resorbed and patchily zoned, with or without associated melt inclusions. The resorption zones often fill the entirety of the crystal (Fig. 7a–c, h, i and k), but can also be concentrically distributed (the core and an outer zone frequently; Fig. 7e), or affect only the outer part of the crystal, preserving non-patchy, melt inclusion-free zones in the interior (Fig. 7f). Some crystals with fewer melt inclusions show concentric oscillatory zoning in which zones are convolute or rounded and irregular in width (Fig. 7g and j). Rare oscillatory-zoned crystals with faceted zones are melt inclusion-free and were observed in the lavas only (Fig. 7l).

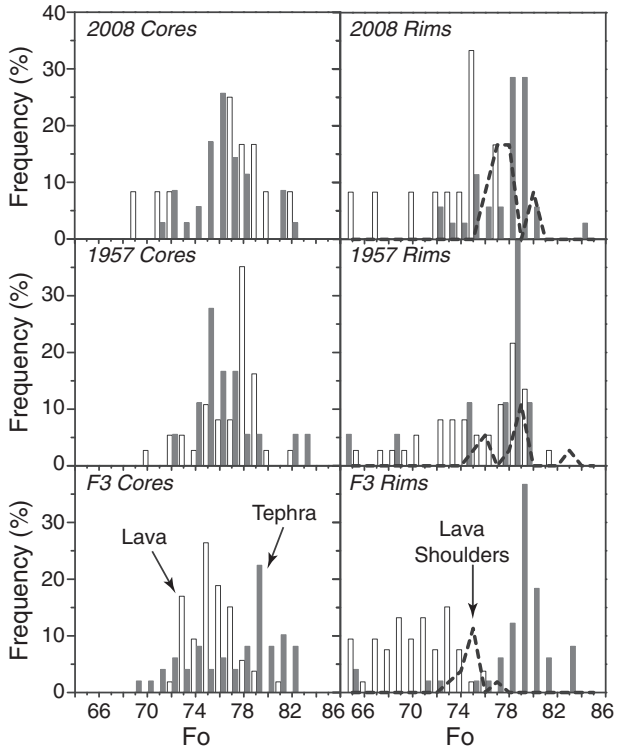

Fig. 6. Histograms comparing the core (left) and rim (right) compositions of olivines from the lavas (white) and tephra (gray). Cores span a similarly large range in composition, suggesting common sources. Rims of olivines from the tephra and reversely zoned shoulders of olivines from the lavas span a similarly narrow range in Fo content, whereas rims of olivines from the lavas are shifted toward a large range of lower Fo contents. The systematic convergence of rim compositions in the olivines from the tephra is interpreted as the assemblage and homogenization of multiple magma batches prior to eruption. The same can be interpreted for the reversely zoned shoulders of the olivines from the lavas; however, the assemblage and homogenization was not as thorough, considering that reversely zoned shoulders are not systematically present.

Texturally distinct zones can be identified in the cores and rims of most crystals, and they have received particular attention to pinpoint general processes that affected the whole crystal population. A schematic representation of a fictive plagioclase phenocryst containing all of these typical features is shown for reference in Fig. 7. Internal parts of the crystals display three characteristic textures that are sometimes combined within a single crystal (Fig. 7a–f). (1) Large, An-poor (low BSE intensity; i.e. dark) zones occur in the core (Fig. 7a) or frequently surround texturally distinct central zones (Fig. 7c–f). They are referred to as An-poor cores. (2) An-rich (bright) zones that are extremely patchy, almost wormy, frequently occur within the central parts of the crystals (Fig. 7b and e), sometimes surrounding texturally distinct cores (Fig. 7a). They are referred to as wormy An-rich cores. (3) Rare An-rich (bright) skeletal zones that are not wormy occur as single crystals or cores surrounded by subsequent plagioclase overgrowth (Fig. 7c and f). These are referred to as skeletal An-rich cores.

A minimum of one resorption zone can be observed in all plagioclase crystals, except for the rare oscillatory-zoned crystals with faceted zones that were observed in the lavas only. The outermost resorption feature recorded in a crystal received specific attention and is referred to as the outermost resorption zone or ORZ. It ranges from a narrow and convolute An-rich (bright) zone (Fig. 7g) to a major patchy zone filling the whole crystal (Fig. 7h, i and k), but it always corresponds to the resorption feature closest to the rim. Because it is a resorption feature, it is heterogeneous by nature, often including interwoven melt inclusions with intricate low- and high-An patches (Fig. 7h, i and k).

External parts of the plagioclase phenocrysts are subdivided into two concentric zones; an inner rim (INR) and an outer rim (OUT). The inner rim comprises the non-resorbed overgrowth zone(s) surrounding the ORZ. It is never patchy and often shows oscillatory zoning (Fig. 7g–i and k), but can be homogeneous when narrow (Fig. 7a). The outer rim is non-resorbed as well, resembles associated microlites in composition (same BSE intensity), and often displays rapid crystallization textures such as swallow-tail prolongations of the crystal corners (Fig. 7b, k and l). Inner and outer rims are better developed in the lavas than in the tephra, where outer rims are narrow and inner rims are sometimes absent.

Plagioclase compositions

Plagioclase crystals have similar major and trace element compositions in lavas and tephra deposits. Point analyses in plagioclase crystals delimit a large range in anorthite content ($An_{53–93}$), Sr concentration (700–1500 ppm), and Fe concentration (3500–10 000 ppm). Whereas Sr is constant within error (±320 ppm) and shows no correlation with An content, Fe displays a slight negative correlation with An content. Exceptionally high concentrations of Fe occur only in plagioclase rims. Owing to the large interaction volume of X-rays in plagioclase and the high atomic weight of Fe, fluorescence can easily affect the measurement of Fe in plagioclase if an iron-rich phase is present at a short distance below the point of analysis. Longhi *et al.* (1976) and Sugawara (2000, 2001) have observed that fluorescence effects were frequent within 10–50 μm from the rim. Detailed zoning profiles in a few crystals with only minor resorption features show a slight increase in Fe at the rim (~1000 ppm) with no change in An for some traverses (Fig. 8e and i). This feature would be characteristic of such fluorescence effects. However, other traverses display much larger variations in Fe at the rim that are correlated with variations in An (Fig. 8d, g, h, j and l), which suggest that the measured Fe concentrations in these traverses are meaningful. This inference is

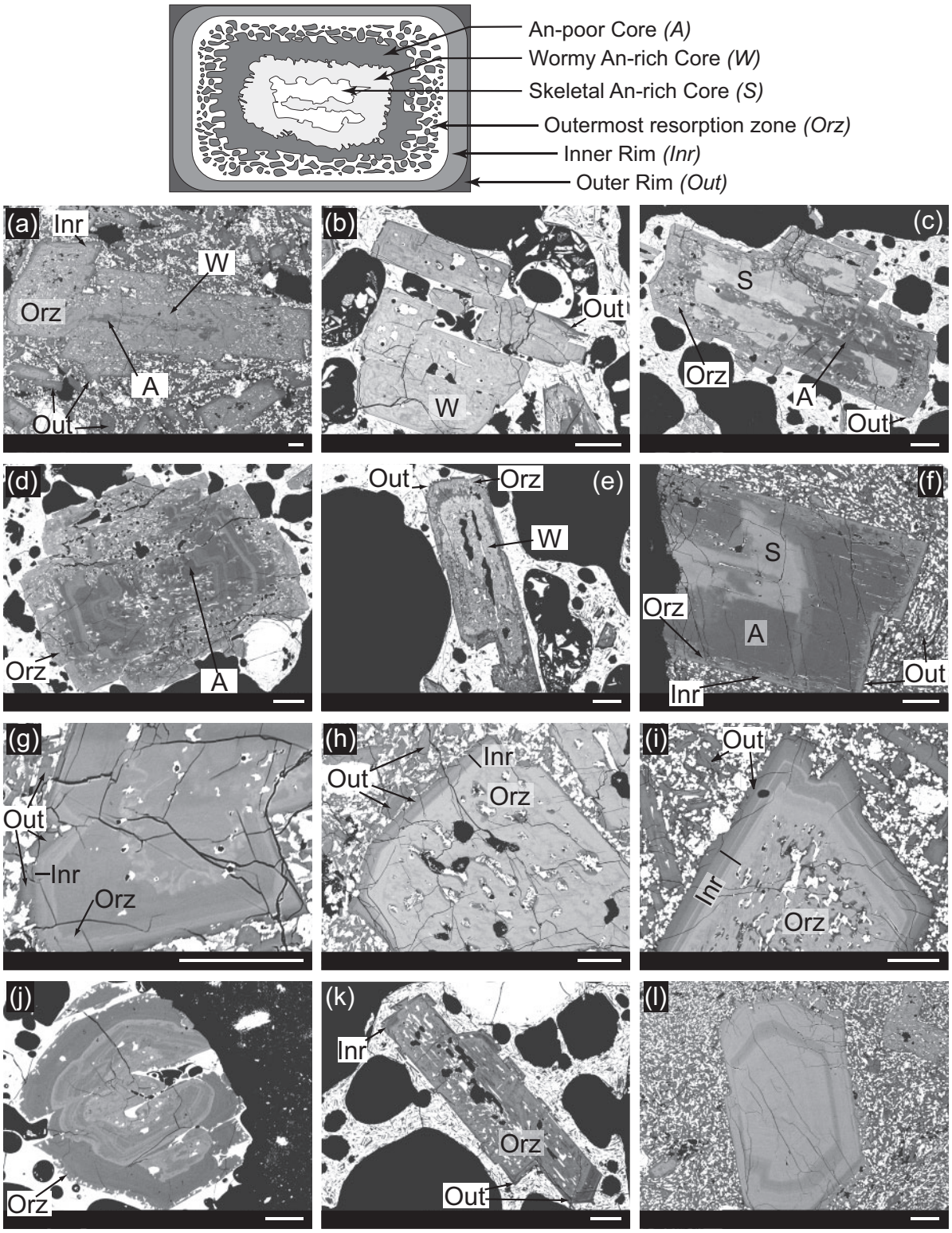

Fig. 7. Top, schematic representation of a fictive plagioclase crystal displaying a combination of all the textural features discussed. Bottom, selection of representative plagioclase phenocrysts from the lavas and tephra displaying characteristic core and rim textures, and their spatial distribution. The scale bar represents 100 μm. BSE images (a, f, g–i, l) are images of crystals from the lavas and (b–e, j, k) of crystals from the tephra, hence the much glassier matrices. The upper six BSE images are good examples of the core textures and their locations within crystals.

(continued)

supported by the fact that Mg and Ti, which are negligibly affected by fluorescence, are positively correlated with Fe and correlate similarly with An content (Fig. 8a, c and l). We consider that the high Fe concentrations measured at the plagioclase rims are pertinent to an understanding of magmatic processes and are not systematically due to fluorescence.

Relating textural zonations to compositional variations

The texturally distinguishable core features form clusters on Fe versus An plots (Fig. 9). An-poor cores typically have low An ($An_{55–65}$) and moderate Fe concentrations (4500–5500 ppm), whereas wormy An-rich cores have higher An contents ($An_{80–85}$) for similar Fe concentrations. Skeletal An-rich cores define yet another cluster with higher An contents ($An_{85–95}$) and lower Fe concentrations (≤4000 ppm) compared with wormy An-rich cores.

The outermost resorption zones, inner rims, and outer rims define a continuum from high An contents and moderate Fe concentrations in ORZs ($An_{80–85}$, 4500–5500 ppm Fe) to low An contents but high Fe concentrations in outer rims ($An_{55–65}$, ~10,000 ppm Fe; Fig. 9). The compositions of these three zones overlap and vary from one crystal to another in each sample. ORZs, the compositions of which are similar to wormy An-rich cores, always have moderate Fe concentrations (4500–5500 ppm), but can display a range in An contents from An_{85} almost down to An_{65}, depending on where the composition was analyzed in the patchy zone. The An contents of inner rims overlap with those of ORZs in the tephra, but are shifted toward lower An contents in the lavas (Fig. 9). In both lavas and tephra, the compositions of inner rims extend to slightly higher Fe concentrations than those of ORZs. Outer rims generally have low An contents (≤An_{70}) but can reach extremely high Fe concentrations (~10 000 ppm). Compositions of outer rims prolong the decreasing An content and increasing Fe concentration trend defined by the inner rims and some ORZs of plagioclase from lavas. On the other hand, the transition from inner to outer rims in plagioclase from the tephra is less continuous. More analyses of outer rims were obtained for the lavas than the tephra owing to the small widths of outer rims in the tephra samples that often prevented analysis. Rare analyses of microlites in the lavas were added to the outer rim group because of their striking textural and compositional resemblance, whereas no analyses of microlites were obtained for the tephra because of their small size.

MAGMATIC PROCESSES AND EVENTS RECORDED BY MINERAL PHASES

Processes recorded by plagioclase

The major element composition of plagioclase (i.e. An content) depends on a number of variables including magma composition, pressure, temperature, and dissolved water content (Housh & Luhr, 1991; Nelson & Montana, 1992; Sisson & Grove, 1993; Couch *et al.*, 2003*a*, 2003*b*). Magma crystallization and differentiation will drive plagioclase toward less An-rich compositions, whereas an increase in magma temperature or water content will promote the crystallization of more An-rich compositions. The effect of pressure on plagioclase composition is less pronounced than that of temperature [an increase of <2 mol % An per kbar was observed by Housh & Luhr (1991) and Nelson & Montana (1992)]. A continuous change in the environmental conditions will induce smooth changes in the plagioclase composition, in the form of continuous, euhedral, oscillatory zoning patterns. Abrupt changes in the environmental conditions will lead to significant disruptions in crystal zoning patterns through dissolution of the disequilibrium composition and quasi-simultaneous re-precipitation of the new equilibrium composition (Nakamura & Shimakita, 1998; Ginibre *et al.*, 2002; Landi *et al.*, 2004; Ginibre & Worner, 2007; Ruprecht & Worner, 2007; Streck, 2008). Resultant resorption textures are dusty or sieve-like, preserving small patches of the previous plagioclase and melt inclusions formed by partial melting of the crystal, associated with small patches of the newly grown plagioclase (Tsuchiyama, 1985). The widespread occurrence of such intense resorption features in Llaima plagioclase phenocrysts (patchy zoning, dense melt inclusion populations) suggests that most crystals experienced at least one, but more often multiple major changes in their crystallization environment. The injection of a mafic magma into a reservoir will create an abrupt change in magma composition and an increase in temperature and water content of the crystallizing liquid, thereby favoring extensive plagioclase resorption.

Fig. 7 Continued
An-poor cores can be central (a, d) or surround other textures (c, e, f); wormy An-rich cores can also be central (b, e) or surround other textures (a), and skeletal An-rich cores are always central (c, f). The following three BSE images (g–i) are good examples of rim textures. All images were taken from lavas because of the better developed inner and outer plagioclase rims. The lower three BSE images are examples of the general variability of textures observed in plagioclase, with oscillatory-zoned crystals in which zones are convolute (j), intensely resorbed crystals with rapid growth outer rims suggested by swallow-tail prolongations of the crystal corners (k), and rare oscillatory-zoned plagioclase with euhedral, faceted zones found in the lavas only (l). The left-hand column of BSE images (a, d, g, j) is ordered to illustrate a downward decrease in the resorption intensity of the outermost resorption zone.

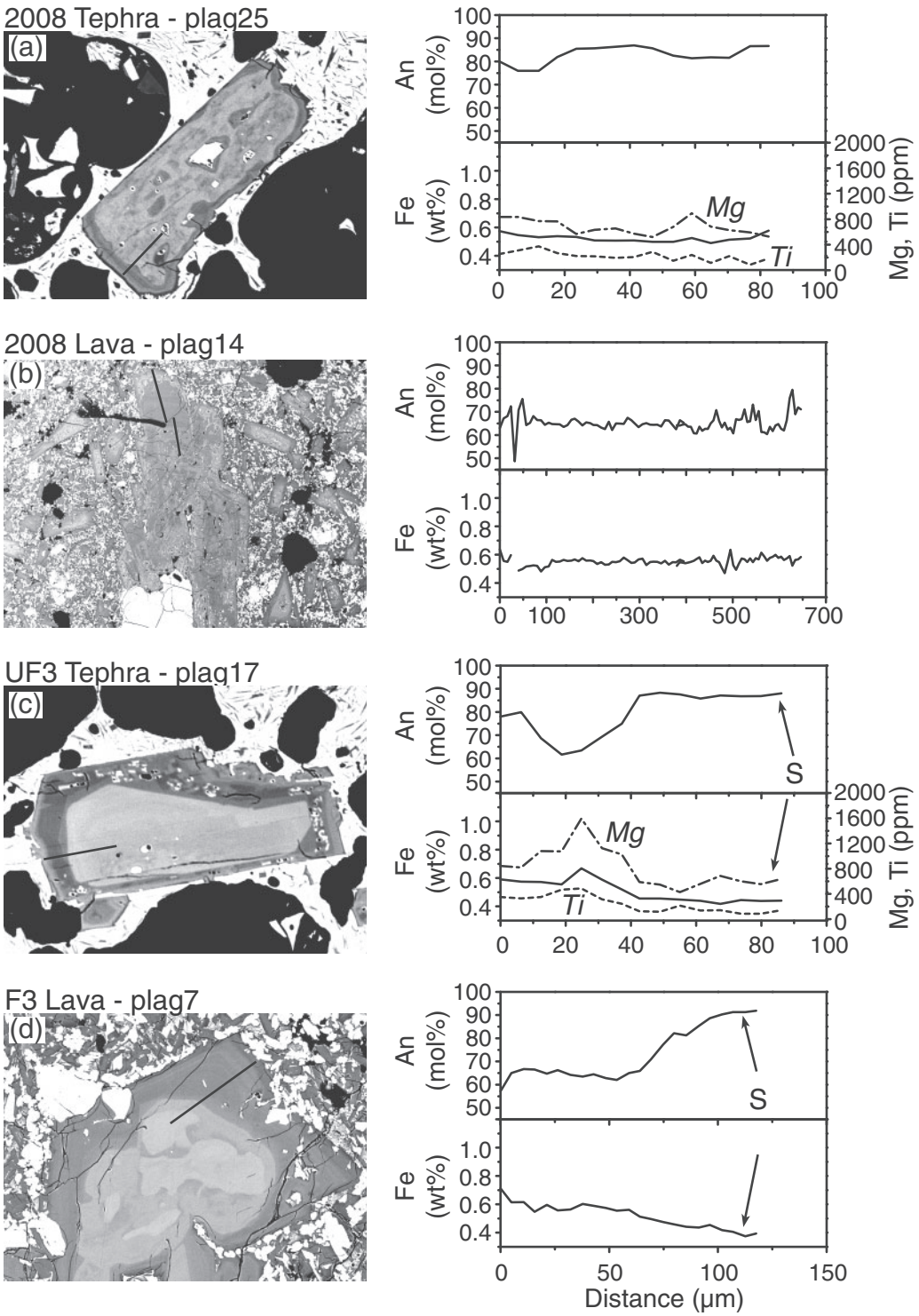

Fig. 8. An, Fe, and occasional Mg and Ti zoning profiles in the few plagioclase crystals that were sufficiently devoid of melt inclusions to allow this type of measurement. In some rare crystals, Fe concentration slightly increases at the rim associated with no change in An content (e, i). This feature is potentially indicative of Fe fluorescence during analysis. However, in most cases, Mg and Ti behave similarly to Fe and are inversely correlated with An content in skeletal An-rich cores (labeled 'S') and at the rims (d, g, h, j, l). These features instead record magmatic processes. Elsewhere in the crystals, Fe, Mg, and Ti are constant whereas An can vary by up to 10 mol %.

(continued)

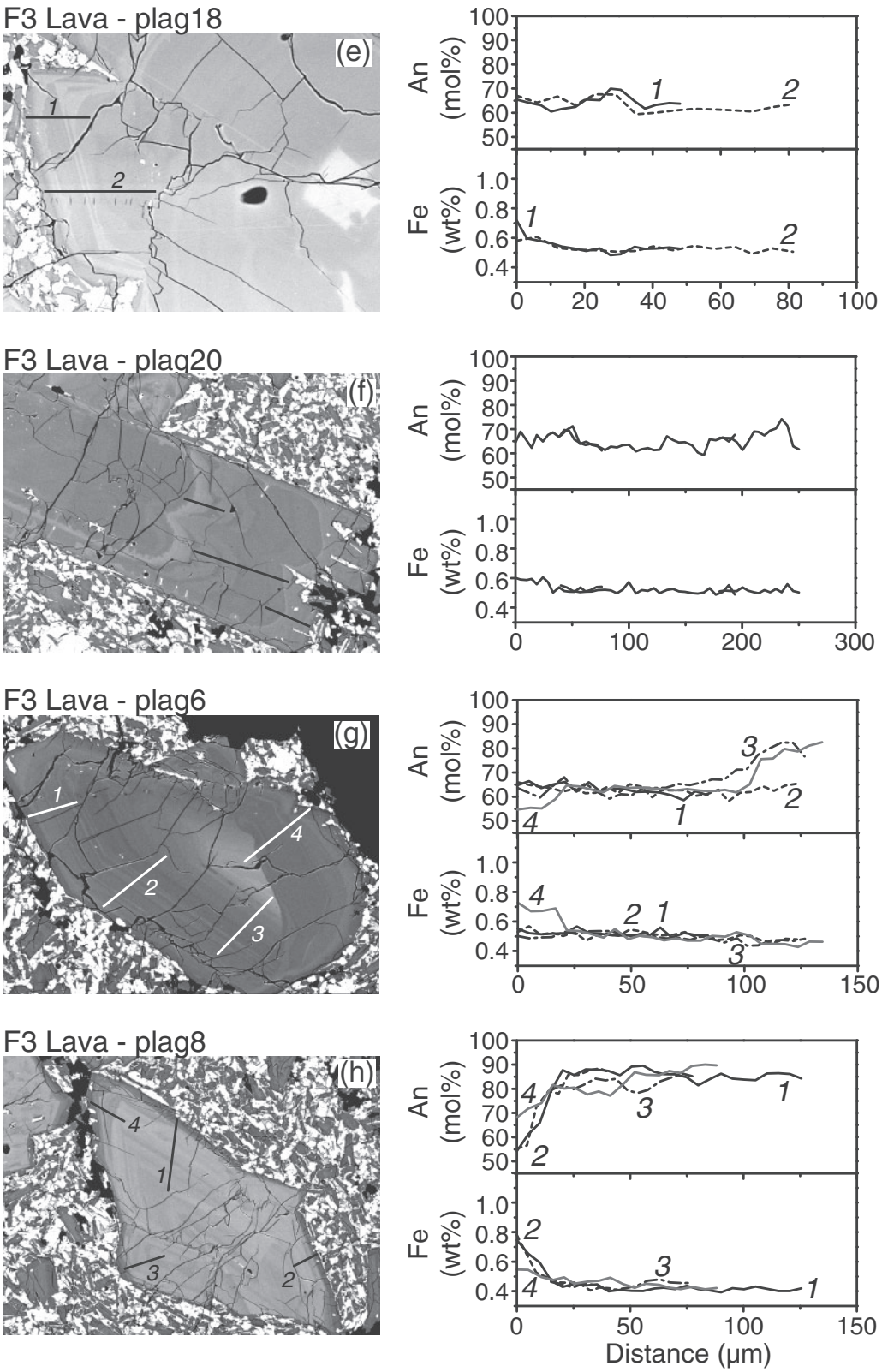

Fig. 8. Continued.

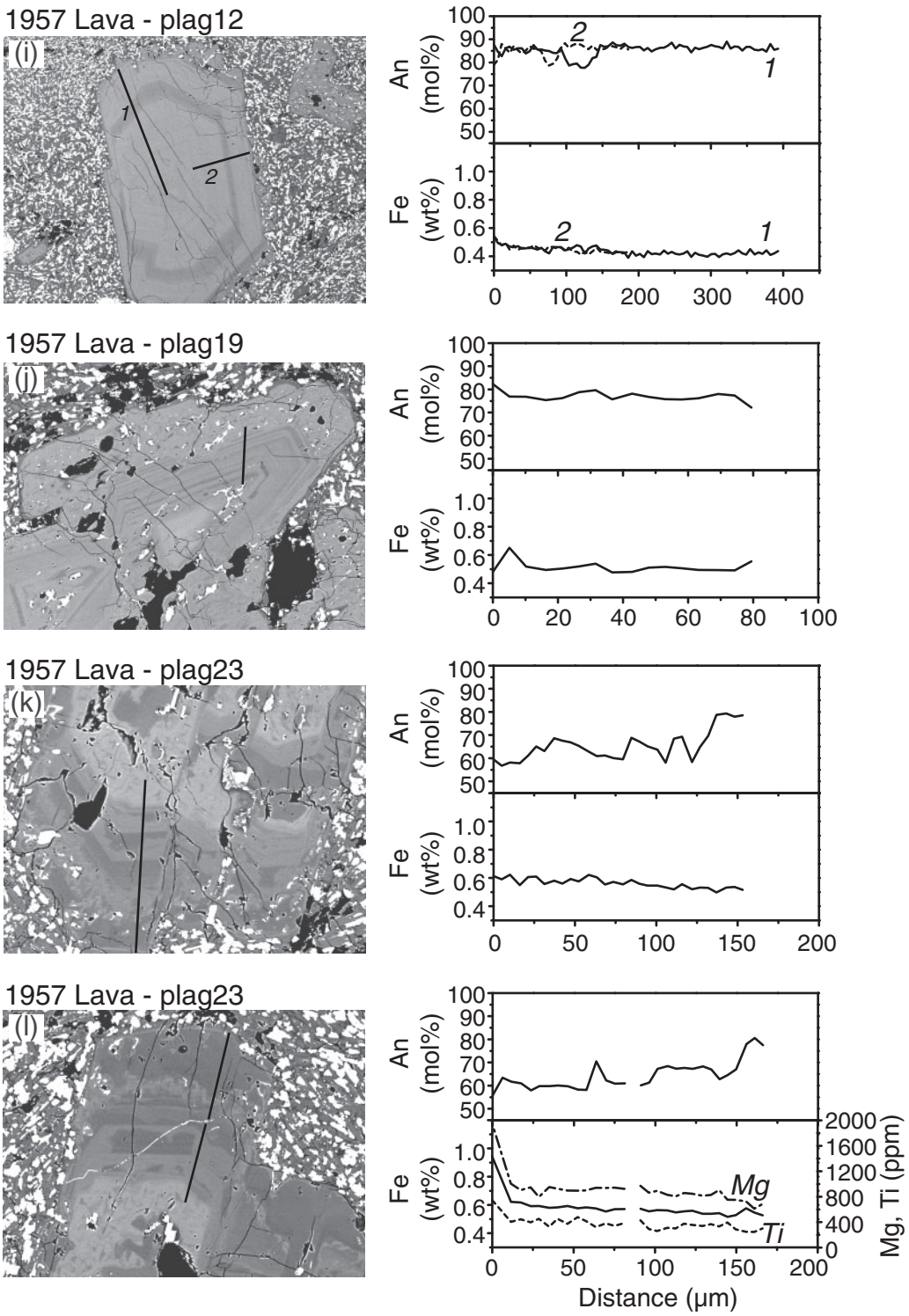

Fig. 8. Continued.

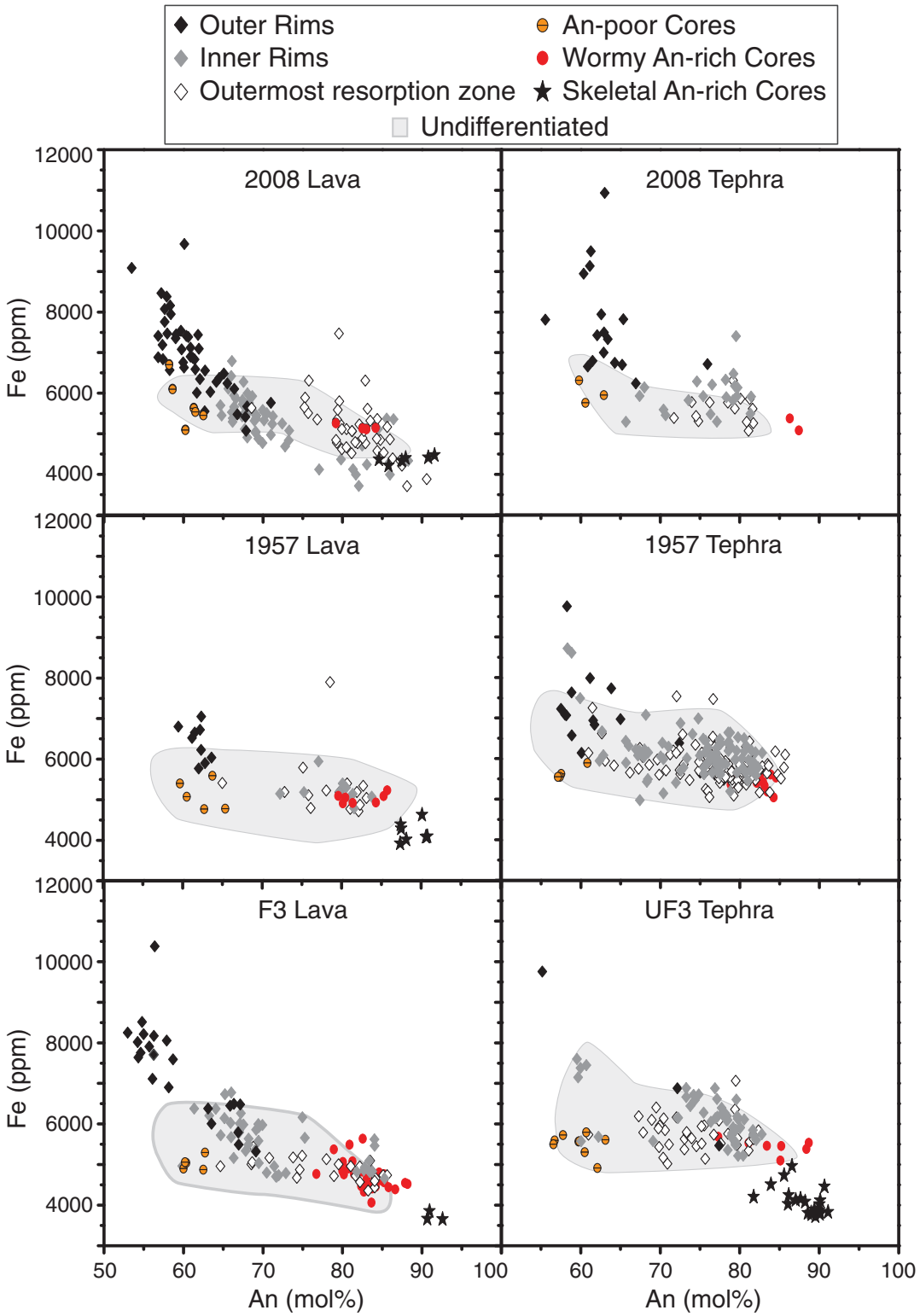

Fig. 9. Fe–An plots for plagioclase from the lavas (left) and tephra (right). Texturally distinguishable core and rim features are also compositionally distinguishable. Tephra and lavas show identical compositions, except for inner rims, which are shifted toward lower An contents in the plagioclase from the lavas than those from the tephra. Skeletal An-rich cores were not analyzed in the 2008 and 1957 tephra. Errors are of the order of ±350 ppm Fe.

Trace elements in plagioclase provide additional constraints on the processes that cause a change in major element composition, as their concentrations in these crystals depend on a different set of variables. Incompatible trace elements such as Fe, Mg, and Ti can also be affected by disequilibrium crystallization processes, and thereby give information on the kinetics of crystallization. Llaima magmas, being stored at shallow depths (≤4 km beneath the base of the edifice; Bouvet de Maisonneuve *et al.*, 2012), define liquid lines of descent that approximate tholeiitic differentiation trends, which is unusual in a continental arc setting. They are characterized by increasing Fe and Ti contents over the compositional range considered (49–60 wt % SiO_2; Fig. 4). Low Fe concentrations in plagioclase, therefore, most probably reflect precipitation from relatively primitive magma compositions.

More or less constant Fe concentrations in the plagioclase cores, in the presence of An variations, can be explained by equilibrium with the long-term composition of the crystal mush, which is controlled by magma mingling and mixing within a system of multiple reservoirs and a high frequency of recharge events. On the other hand, extremely high Fe concentrations are registered at the rims, in association with low An contents (Figs 8 and 9). Fe partitioning strongly depends on melt and plagioclase composition, temperature (Sugawara, 2001), and fO_2 (Longhi *et al.*, 1976; Sugawara, 2001; Aigner-Torres *et al.*, 2007). Such an abrupt increase in Fe would imply either (1) interaction with an extremely evolved magma whose composition was not recorded elsewhere in plagioclase, (2) a very sharp decrease in temperature, (3) a very sharp increase in oxygen fugacity, or (4) fast, out-of-equilibrium crystallization. Ti and Mg seem to behave similarly to Fe in the cores and especially in the outer rims (i.e. extremely high concentrations at the rim compared with the core; Fig. 10). Mg partitioning depends only weakly on temperature (Longhi *et al.*, 1976; Aigner-Torres *et al.*, 2007) or An content (Bindeman *et al.*, 1998), and Ti essentially depends on temperature (Bindeman *et al.*, 1998; Aigner-Torres *et al.*, 2007). Neither depends on melt composition or fO_2. Therefore, changes in these variables are not responsible for the correlated increases in Fe, Mg, and Ti at rims. A sharp decrease in temperature is not what would be expected just prior to eruption and is not what is recorded by reversely zoned olivine crystals in tephra (Bouvet de Maisonneuve *et al.*, 2012), implying that a decrease in temperature can also be ruled out as the cause of these variations. We propose that the sharp increases in these elements are due to rapid disequilibrium crystallization during eruption, from boundary layer melts enriched in Fe, Mg, and Ti. If diffusion of these incompatible elements out of the boundary layer melt is not rapid enough, they will be incorporated excessively by rapidly crystallizing plagioclase (Albarède & Bottinga, 1972). Rapid crystallization of the rims is in agreement with the observation of swallow-tail prolongations of crystal corners (Lofgren, 1980).

Combining textural information with major and trace element variations in plagioclase phenocrysts allows an interpretation of distinct zones of the cores and rims in terms of specific processes and events that occur at depth below Volcán Llaima. The corresponding dynamics of magma storage, crystallization and recharge are schematically summarized in Fig. 11.

(1) An-poor cores formed in the evolved mush present at shallow depths below the volcanic edifice. They formed after significant degassing, cooling and crystallization at low pressures, hence the low An contents and moderate Fe concentrations.

(2) Skeletal An-rich cores that crystallized from a parent or recharge magma are identified by extremely low Fe concentrations and high An contents. Their coarse skeletal textures resemble resorption textures produced experimentally by rapid decompression in a water-undersaturated environment [compare Fig. 7c and f with figs 1 and 5 of Nelson & Montana (1992)]. These were brought from depth to shallow magma reservoirs during mafic recharge events, and represent the very rare witnesses of crystallization at depth from relatively primitive magmas (Fig. 11a).

(3) Wormy An-rich cores correspond to the resorption of An-poor cores during an early magma recharge event (Fig. 11b). They resemble resorption textures obtained experimentally by chemical disequilibrium [compare Fig. 7a, b, and e with fig. 4 of Nakamura & Shimakita (1998) or fig. 2 of Tsuchiyama (1985)], but contain fewer melt inclusions owing to healing through extended crystallization. Their Fe concentrations are similar to those of An-poor cores, which is consistent with simultaneous re-precipitation of new plagioclase from the local melt pockets formed during dissolution of pre-existing plagioclase (Tsuchiyama, 1985; Nakamura & Shimakita, 1998). Very little to no interstitial (i.e. matrix) melt is directly involved in the process.

(4) Outer resorption zones correspond to the resorption of An-poor cores during the last magma recharge event (Fig. 11c). An contents and Fe concentrations strongly resemble those of wormy An-rich cores (although An contents span a larger range) and resorption textures also resemble those obtained experimentally by chemical disequilibrium [compare Fig. 7a, h, and i with fig. 4 of Nakamura & Shimakita (1998) or fig. 2 of Tsuchiyama (1985)]. Melt inclusions are numerous and healing of the resorption zone through extended crystallization is not observed, implying that the eruption occurred shortly after magma recharge. ORZs span a large range in An contents owing to the intricate association of newly crystallized plagioclase with remnants of the pre-existing plagioclase. Once again, Fe concentrations are moderate and similar to those of An-poor cores owing to the

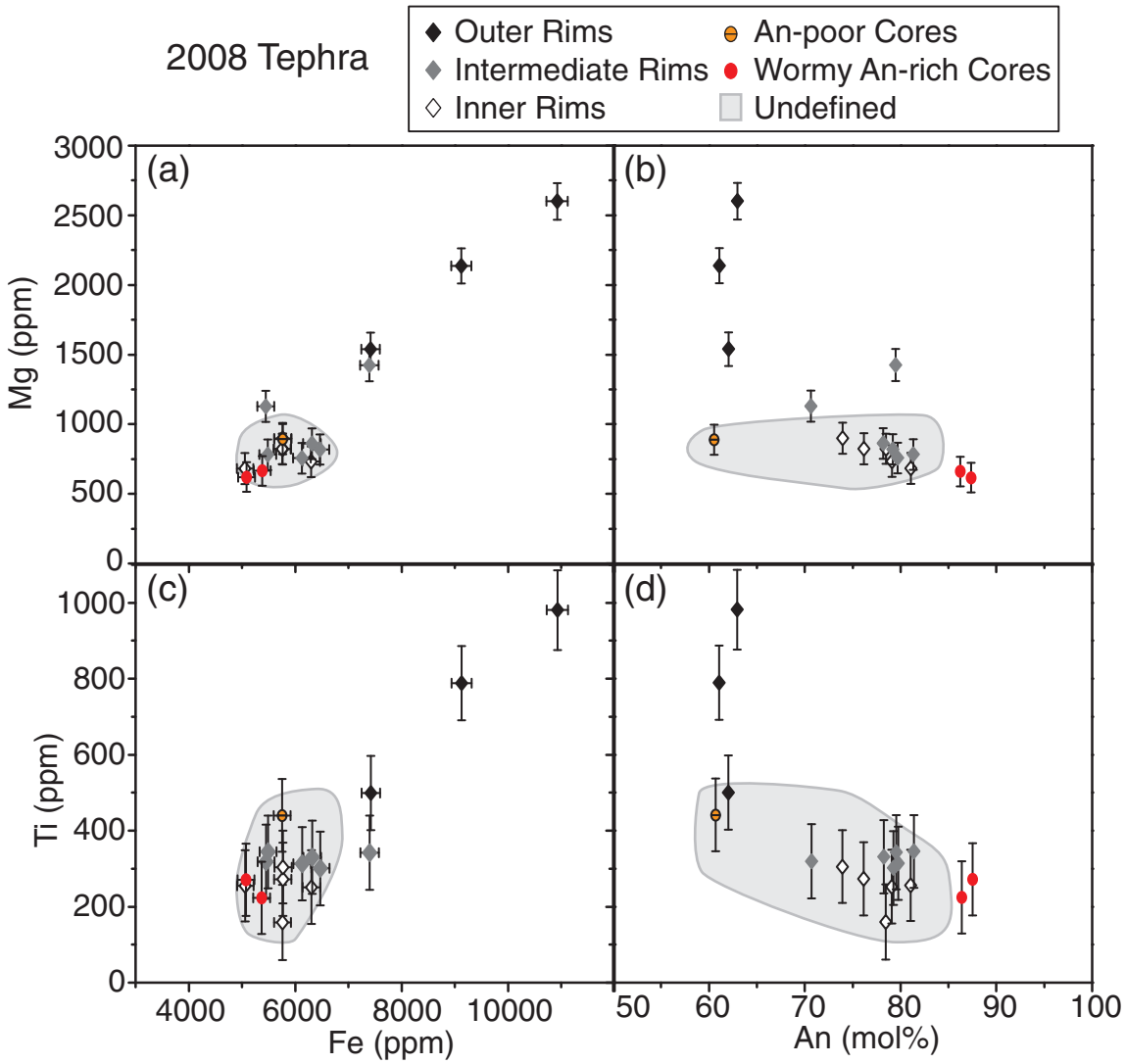

Fig. 10. Mg and Ti as a function of Fe (left) and An content (right) in plagioclase crystals from the 2008 tephra. Mg and Ti are linearly correlated with Fe and display the same variations as a function of An content for the different textural zones of the cores and rims. Such correlations imply that high Fe concentrations at plagioclase rims are the product of rapid growth during eruption rather than fluorescence during analysis.

simultaneous re-precipitation of new plagioclase from local melt pockets formed during resorption of pre-existing plagioclase. Very little to no interstitial (i.e. matrix) melt is directly involved in the process.

(5) Inner rims, which are not always present and are sometimes oscillatory-zoned, formed by subsequent crystallization of plagioclase after the last magma recharge event (Fig. 11d). Plagioclase crystallizes according to the local equilibrium composition, and An-rich plagioclase is in equilibrium with a liquid containing a greater volume fraction of recharge magma compared with An-poor plagioclase. Inner rims differ in An content between lavas and tephra (Fig. 12). Inner rims in tephra display a wide range in An contents, reflecting incomplete hybridization between the recharge magma and the resident interstitial liquid. Oscillatory zoning potentially reflects convective mixing that occurred between the recharge magma and the resident mush (Fig. 7g, i and k). Plagioclase crystals in lavas have inner rims that cluster at low An contents (Figs 9 and 12), lower than for the tephra, implying either interaction with a smaller volume fraction of recharge magma or crystallization from a more degassed magma. The trends toward high Fe concentrations in inner rims are suggestive of rapid crystallization. Some analyses of inner rims in the plagioclase from the 2008 lava show Fe concentrations and An contents similar to those of skeletal An-rich cores, suggesting a strong chemical influence of the primitive recharge magma in this case (Fig. 9).

(6) Outer rims were formed by rapid disequilibrium crystallization during eruption (Fig. 11e). Fe concentrations

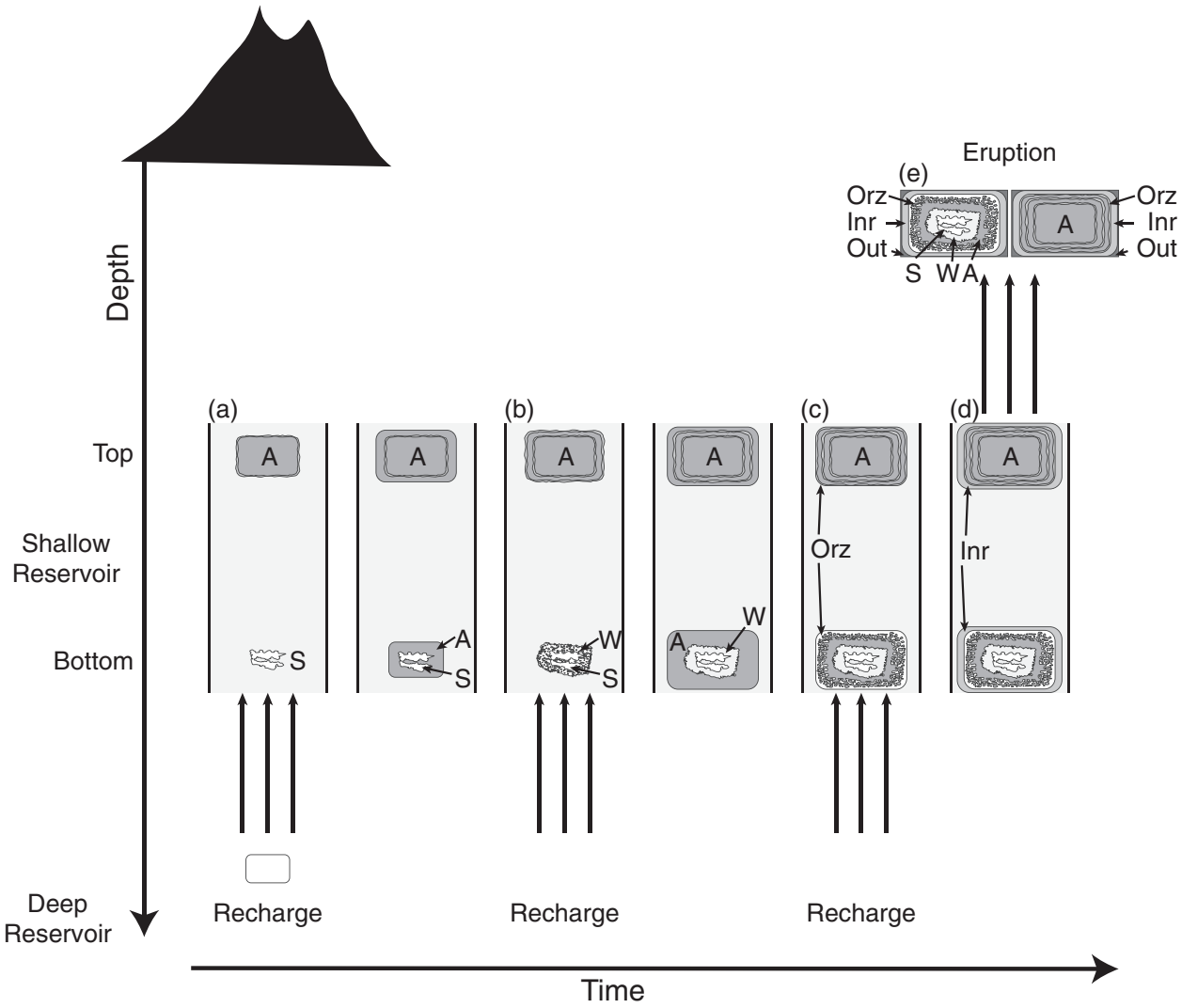

Fig. 11. Schematic representation of magma crystallization, recharge, and eruption processes recorded by plagioclase phenocrysts. For clarity, only one vertical reservoir is considered here. Gray scale is intended to mimic the BSE intensity observed on scanning electron microscopy images. The labels A, S, W, Orz, Inr, and Out stand for An-poor core, skeletal An-rich core, wormy An-rich core, outermost resorption zone, inner rim and outer rim respectively. Magmas are dominantly stored in shallow dike-like reservoirs and crystallize An-poor (dark) plagioclase during mush formation (labeled A). (a) Injection of a mafic magma from a deeper reservoir can introduce An-rich cores (bright) into the shallow reservoir. These cores are resorbed and become skeletal as a result of decompression of the water-undersaturated recharge magma (S). The resident mush plagioclase is also resorbed owing to a change in liquid composition and/or the supply of heat and volatiles. Crystallization of An-poor plagioclase around the skeletal An-rich cores and the resorbed mush crystals will occur during a period of quiescence between two magma recharge events. (b) A subsequent injection of mafic magma in the system will destabilize the newly crystallized An-poor plagioclase. Crystals at the base of the reservoir are probably more affected than those at the top owing to direct mixing with the recharge magma (W). Again, crystallization of An-poor plagioclase will occur during a period of quiescence, and the resorbed zones may 'heal' their melt inclusions through prolonged crystallization. (c) The last magma recharge event prior to eruption will destabilize the outer An-poor zones of plagioclase crystals, forming texturally distinguishable outer resorption zones (Orz). (d) The short time available between magma recharge and eruption allows crystallization of an unresorbed inner rim (Inr), the composition of which will be controlled by the composition, temperature, and volatile content of the hybrid magma present in the reservoir. During magma ascent in the conduit, rapid plagioclase growth takes place, forming the microlite population and the outer rims of the phenocrysts (e, Out). All Llaima plagioclase phenocrysts do not record three recharge events; some may preserve the evidence for more events, others for fewer.

and An contents reflect kinetic effects rather than magma composition, temperature, or water content. The effect of disequilibrium crystallization on the major element compositions of plagioclase crystals will be to favor An-poor compositions, as Ca—a compatible element—is depleted in the boundary layer melt. Additionally, magma degassing during eruption will drive plagioclase to lower An contents. This is in agreement with the correlation of low

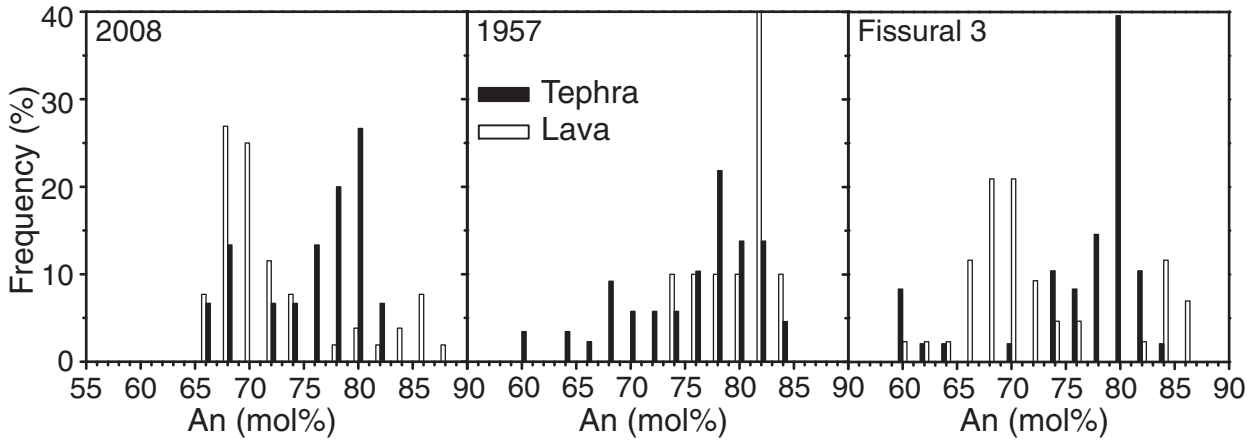

Fig. 12. Comparison of the An contents of inner rims in plagioclase from the lavas and tephra showing globally lower An contents for the lavas than for the tephra. Inner rims of crystals from the tephra must have grown from a globally warmer, more mafic, and/or more volatile-rich magma than those from the lava. The 1957 eruptive episode, however, displays similar An contents for the inner zones of the plagioclase from the lavas and tephra.

An contents with high Fe concentrations and similar trends measured in the lava microlites.

Assembling the information given by plagioclase and olivine

The plagioclase textures and compositions of lavas and tephra can readily be explained by processes and events that were inferred from olivines and their melt inclusions (Bouvet de Maisonneuve *et al.*, 2012). Compositional trends defined by evolved olivine-hosted melt inclusions were inferred to be the result of shallow evolution of interstitial melt during the formation of crystal mush bodies, as a consequence of degassing and crystallization. The widespread occurrence of An-poor zones, either physically (An-poor cores) or cryptically through the presence of resorption zones implying an anterior less An-rich plagioclase composition (wormy An-rich cores, ORZ), suggests that Llaima magmas dominantly produce An-poor plagioclase, which is consistent with degassing and crystallization in a shallow reservoir.

The ranges in olivine core compositions in single thin sections and the absence of correlated H_2O–CO_2 degassing and magma evolution trends have been interpreted to be due to magma storage in multiple vertically extended reservoirs. The existence of vertically extended reservoirs is supported by the range in plagioclase textures for a single eruptive event. The intensity of resorption of the ORZs, which record the last recharge event, varies from (1) crystals that were entirely resorbed to the core (Fig. 7a and k), to (2) crystals that were extensively resorbed but preserved a few low-An remnants in their cores (Fig. 7d), (3) crystals that display narrow (a few microns wide) resorption zones right at the rim (Fig. 7e and f) or (4) display slightly wavy interfaces between old An-poor cores and new An-rich inner rims (Fig. 7g), and (5) crystals that only show a few melt pockets and embayments right at the rim (Fig. 7j). The extent of resorption through dissolution and re-precipitation depends on the magnitude of the environmental change, the dimensions of the disequilibrium plagioclase zones, and the time available for such a process to occur (Tsuchiyama, 1985). Recharge events will strongly affect crystals that physically interact with the mafic magma injection and therefore experience a change in composition, temperature, and water content of the host liquid, but will less affect crystals that experienced only a change in temperature and/or water content of the liquid owing to heat conduction or volatile diffusion through the resident crystalline magma. Mafic magma injections into vertically extended reservoirs will progressively mix with and percolate through the overlying mush bodies, strongly resorbing crystals at the base of the reservoir and having a lower impact on crystals at the top (Fig. 11a–d). Eruptions sample the reservoir in this variable state and prevent any further resorption; hence the diversity in resorption textures visible in single hand specimens (Fig. 11e).

The occurrence of frequent, but small-volume, recharge events is supported by the numerous resorption zones of variable magnitude recorded by plagioclase cores (Fig. 11b). These frequent injections of more primitive magma are essential to maintain the bulk of many crystal mush-filled dikes located at shallow, upper crustal levels in an eruptible state. Long-term compositional homogeneity, such as that at Llaima, is frequently observed at hyper-active mafic volcanoes, such as Stromboli, Italy (Landi *et al.*, 2004), Arenal, Costa Rica (Streck *et al.*, 2005), or El Chichón, Mexico (Andrews *et al.*, 2008). This suggests that a long-term balance between magma recharge, crystallization, and eruption is reached at these highly active volcanic systems.

The preponderance of reversely zoned olivines in tephra suggests that eruptions are triggered by the injection of mafic magma into the shallow reservoirs. This mafic recharge event is also recorded by plagioclase phenocrysts in the shape of An-rich ORZs. The overall agreement between the plagioclase and olivine mineral records supports the previously proposed model (Bouvet de Maisonneuve *et al.*, 2012) and allows further interpretations of eruption dynamics.

Timing and location of crystallization

Three temporally distinct crystallization periods can be distinguished: (I) crystallization in the magma chamber during repose periods and early magma recharge events; (II) crystallization in the magma chamber after the latest, potentially eruption-triggering replenishment event; (III) crystallization during magma ascent and eruption. ORZs in plagioclase record the last recharge event and therefore mark the limit between periods I and II. A similar threshold can be defined in the olivine crystals at the transition from non-zoned cores to normally or reversely zoned rims.

Crystallization during ascent and eruption is marked by kinetic effects such as disequilibrium compositions owing to rapid cooling and decompression. Microlites and outer rims of plagioclase show rapid growth textures associated with extremely high Fe concentrations and low An contents. Similarly, outermost rims of olivines from the lavas show extremely low Fo contents and a variety of rim compositions, reflecting disequilibrium crystallization from a boundary layer melt or in a highly crystalline environment. This feature is not present in the olivines from the tephra, implying that magma ascent and eruption was too rapid to allow olivine crystallization. Given that late, syn-eruptive crystallization is responsible only for the presence of microlites (~20 μm in diameter) and well-developed outer rims (~10–40 μm wide) in millimeter-sized plagioclase and olivines from the lavas, the arbitrarily chosen threshold at ~40 μm effectively distinguishes between phenocrysts that essentially grew in the magmatic reservoirs and microlites that grew during magma ascent to the surface. The dimensions of the long axes of all crystals present within a representative area of a thin section were measured (1000–2000 crystals per sample in the tephra and 2000–4000 crystals in the lava), and curves of the cumulative percentage of crystals within a given size range overlap well for lava and tephra produced during a same eruptive event (see Appendix Fig. A1). We can therefore consider that reported phenocryst contents approximate pre-eruptive magma crystallinities.

Information on immediately pre-eruptive, magma chamber dynamics is preserved in the zones intermediate between the older cores and the rapidly crystallized outermost rims; that is, in the inner rims of plagioclase and the zoned shoulders or rims of olivine crystals. The fact that olivine rims are compositionally zoned implies that some time elapsed between magma recharge and eruption, during which Fe and Mg started to diffusively re-equilibrate. The presence of well-developed inner rims in plagioclase phenocrysts from the lavas suggests that more time was available for crystallization between magma recharge and eruption in comparison with the tephra. Assuming a growth rate of 10^{-10} cm s^{-1} (Marsh, 1988; Couch *et al.*, 2003*b*), ~10 μm wide inner rims in plagioclase crystals from the lavas would form in ~100 days, suggesting that lavas are erupted from a few days to weeks after the tephra eruption.

WHAT DOES PETROLOGY TELL US ABOUT ERUPTION DYNAMICS?

Comparing lavas and tephra

Modal abundances of phenocrysts in lavas and tephra are significantly different, with ~15–20 vol. % more phenocrysts in lavas than in tephra (Fig. 3). Considering that phenocryst contents approximate pre-eruptive magma crystallinities, as discussed above, the lower phenocryst contents in tephra relative to lavas suggest a greater dilution of the resident mush by the crystal-poor recharge magma to produce explosively erupted magmas. Mixing proportions of ~70:30 (recharge:mush) for the tephra and ~40:60 for the lavas are required to explain the observed crystallinities, considering a resident mush with 60 vol. % phenocrysts and a recharge magma with 5 vol. % phenocrysts.

Olivine cores from lava and tephra span the same ranges in composition, confirming that they have common origins and crystallized under similar conditions. The main divergence between phenocrysts from lavas and tephra concerns the rim zoning patterns. Convergent olivine rim compositions and the dominance of reversely zoned crystals in tephra suggest assembly, reheating, and homogenization of multiple magma batches just prior to eruption. When present, reversely zoned shoulders in lava olivines converge toward the same reduced range in composition as the olivine rims from tephra (Fig. 6). These crystals, therefore, also have experienced assembly, reheating, and homogenization before rapidly crystallizing during eruption. A fraction of the olivines from the lava, however, have homogeneous cores overgrown by normally zoned rims that crystallized during eruption (particularly noticeable in the Fissural 3 lava). Assembly and homogenization of the olivine populations present in lavas was thus not as complete as in the case of the explosively erupted magma. A smaller volume of recharge magma would be sufficient to explain the partial homogenization of the olivines in the effusive products, whereas a large volume of recharge

magma would be required for all the crystal rims of the explosive products to be systematically affected.

Plagioclase phenocrysts from lavas and tephra are very similar, which again is in agreement with storage in common magma reservoirs. They display the same texturally and compositionally distinct zones in their cores (An-poor cores, skeletal An-rich cores, wormy An-rich cores; Fig. 9), but slight differences in zoning at the rims. The range in An contents of inner rims and their occasional oscillatory zoning is attributed to variable degrees of interaction with the recharge magma (i.e. variable liquid compositions, temperatures, and volatile contents) owing to incomplete hybridization with the resident mush before eruption. Lower An contents in inner rims of plagioclase from the lavas compared with those from the tephra suggest a reduced influence of the recharge magma in the effusively erupted magma. This is supported by the rare presence of non-resorbed, melt inclusion-free, oscillatory-zoned crystals (Fig. 7l) that are present in the lava but not in the tephra and that attest to small fractions of resident mush that did not interact with, nor record, the mafic magma injection prior to eruption. Given the contrasting average An contents of plagioclase produced by the recharge magma (An_{90}) and the resident mush (An_{60}), mixing proportions can be roughly estimated from the bulk composition of the inner rims in plagioclase from tephra (An_{78}) and lavas (An_{68}). These are of the order of ~75:25 (recharge:mush) and ~40:60 respectively, which is in good agreement with mixing proportions obtained from phenocryst contents.

Overall, the differences between tephra and lavas imply more pronounced interactions between the recharge magma and the resident mush for explosively erupted magma than for effusively erupted magma. All tephra phenocrysts record an interaction with hotter recharge magma, whereas all lava phenocrysts do not. Whole-rock compositions of tephra and lavas should differ because of variable proportions of primitive recharge magma. Slight differences are indeed observed with ~0·5–1 wt % less SiO_2 and ~1–1·5 wt % more MgO in the tephra samples than in the associated lavas. However, quantitative estimations of the mixing proportions are difficult as they require knowledge of the bulk composition of the crystalline bodies present at depth. Multiple reservoirs are invoked to explain the range in olivine core compositions, and a large range in evolved melt inclusion compositions is observed within each tephra unit (Bouvet de Maisonneuve *et al.*, 2012). Assumptions can be made regarding the interstitial melt composition (evolved olivine-hosted melt inclusion), the mineral compositions (low-An plagioclase, low-Fo olivine) and modal proportions (~90 vol. % plagioclase and 10 vol. % olivine); however, the number of free parameters is such that no reliable mixing proportions could be obtained. Given that the recharge magma is nearly aphyric and its compositional contrast with the resident crystal mush is small, the only way of identifying its presence is through observations of small differences in phenocryst textures and rim compositions between lavas and tephra. We propose that explosive eruptions resulted from cases in which the volume fraction of recharge magma was large, which systematically affected the phenocryst rims and strongly diluted the resident mush. Effusive eruptions, on the other hand, were triggered by smaller volume fractions of recharge magma with respect to the erupted mush, which partially affected the phenocryst rims and only weakly diluted the resident mush.

The volume fraction of recharge magma as a control of eruption style?

Namiki & Manga (2008) studied the transition between fragmentation and permeable outgassing of low-viscosity magmas. They observed from experiments that if the expansion velocity is large enough, the bubbly fluid fragments. Large expansion velocities are favored by low viscosities, high vesicularities, and/or high initial pressures. When a mafic magma injection interacts with the resident crystal mush at Volcán Llaima, the bulk viscosity of the mixture is diminished in comparison with that of the mush, owing to a reduced liquid viscosity at slightly higher temperatures and the dilution of the crystal content. Typical densities and viscosities of ~2550–2580 kg m^{-3} and ~(2–3) × 10^7 Pa s for the mush (59 vol. % plagioclase, 1050°C) and ~2610 kg m^{-3} and ~15–20 Pa s for the recharge magma (3 vol. % olivine, 1145°C) are to be expected at Volcán Llaima, implying a small density contrast between the recharge magma and the resident mush but a viscosity contrast of several orders of magnitude (calculated with Conflow; Mastin, 2002). The dissolved volatile content increases relative to that of the mush, as the recharge magmas have more volatiles than the resident magmas, which have degassed during crystallization at shallow depths. Initial pressures in the reservoir are difficult to estimate, but one would expect them to increase with the volume of magma injected if no magma is simultaneously extruded. Therefore, a large volume of recharge magma would tend to significantly increase the possibility of reaching large expansion velocities and satisfying the fragmentation criterion. This is in agreement with the observation of larger volume fractions of recharge magma in the explosively erupted magma than in the effusively erupted magma. We suggest that shifts in eruption style at Volcán Llaima are due to (1) variable volumes of injected mafic magma during recharge or (2) variable degrees of interaction between resident magmas and recharge magmas.

The amount of recharge magma in a specific erupted body affects its mobility. In the case of a single recharge event characterized by injection into a vertically oriented reservoir, the injected magma progresses through the

central part of the reservoir because it is slightly less crystalline, hotter, and easier to remobilize. Shortly after magma injection, this intensively mixed central part with a large volume fraction of recharge magma will yield a Strombolian paroxysmal type of eruption through the rapid ascent of mobile, gas-rich hybrid magma. The remaining recharge magma will continue to mix with the resident mush, as it starts to degas and crystallize. If magma overpressure in the reservoir is sufficiently high for the eruption to continue, the subsequent erupted magma will be less mobile and less gas-rich, favoring lava effusion.

Magma recharge may also occur as multiple events of minor amplitude. A minimum volume accumulated over a number of injections would be required to remobilize the resident mush and build sufficient overpressure for an eruption to proceed. Once the required volume is attained, a scenario similar to a single recharge event will occur. In both cases, subsequent mafic intrusions would lead to Strombolian paroxysms only if they are voluminous enough to provide the necessary viscosity reduction, vesicularity increase, and/or pressure increase required for elevated expansion velocities and magma fragmentation.

These scenarios are in agreement with the observed 2008 eruptive activity, which started on January 1st with a paroxysmal Strombolian eruption and continued a month later with the extrusion of lava that overflowed from a notch in the summit crater. They are also in agreement with better developed inner rims in the plagioclase phenocrysts from the 2008 lava compared with those from the 2008 tephra (Fig. 7), suggestive of a longer time lapse (some weeks) between magma recharge and eruption, allowing for additional crystallization. During the April 2009 paroxysm, Strombolian explosions and lava effusion occurred simultaneously. If the recharge magma mixes incompletely with the resident mush, the resultant magma can segregate in the vertical, shallow reservoir depending on its local viscosity and crystal content, which in turn induces variable ascent velocities. A possible scenario for the inner workings of the 2009 paroxysm is that the ascent of a phenocryst-poor, volatile-rich magma in the center of the reservoir triggered the Strombolian explosions, whereas the ascent of a phenocryst-rich, degassed magma along the walls of the reservoir, partially entrained by the rapidly ascending magma in the center, generated lava flows.

The phenocrysts from the northeastern 1957 lava flow have very similar textures, compositions, and zoning patterns to those from the 1957 tephra. Olivine compositions strongly converge at the rims (Fig. 5), inner rims in plagioclase overlap in composition with ORZ (Figs 9 and 12), and outer rims are poorly developed. Modal phenocryst abundances, however, remain contrasted, with ~14 vol. % more phenocrysts in the lava than in the tephra (Fig. 3). The northeastern 1957 lava flow differs from the 2008 and Fissural 3 lava flows, and its similarity to the associated tephra suggests that it could have been spatter-fed and not due to an overflow from the summit vent, as was observed for the January 2008 lava flow. A spatter-fed lava flow can be viewed as intermediate between explosive and effusive activity in that magma is effectively fragmented at the vent but not sufficiently to form an ash and scoria-rich plume, as observed during paroxysmal events. Volume fractions of recharge magma greater than those required for lava effusion, but smaller than those required for a paroxysmal eruption, could potentially explain this eruptive style. However, this interpretation remains speculative and would require direct observation from an erupting volcano to be further developed. Inferring the formation mechanism of a lava flow from field observations is often challenging, as complete coalescence of spatter clasts frequently occurs, and single flows may retain little textural evidence of an original clastic origin (Sumner, 1998).

Implications for eruption forecasting

The eruptive style of a given volcanic event at Volcán Llaima appears to be dictated by the vigor of recharge processes that occur in the shallow reservoirs prior to eruption. Our study suggests that the critical condition required for an explosive eruption is the presence of a large volume fraction of recharge magma in the erupted magma, which is controlled by magma mixing and mush remobilization in the shallow reservoir. The volume of remobilized mush and the time scales required for mixing will depend on the crystal content of the mush, the viscosity of the interstitial liquid, the viscosity of the recharge magma, and the way volatiles are redistributed between recharge and mush. The degree of interaction between the recharge magma and the mush will probably vary within a limited range over time at a given volcano, as long as significant changes in mush crystallinity and/or liquid viscosity do not occur. It is probable that a given volume of recharge magma will systematically remobilize a similar volume of crystal mush. Large volumes of recharge magma are potentially recognizable using monitoring tools such as InSAR (Bathke *et al.*, 2011; Chadwick *et al.*, 2011), tilt-meter (Green *et al.*, 2006), or GPS measurements (Jentzsch *et al.*, 2001; Lowry *et al.*, 2001; Geist *et al.*, 2006). Shallow crustal reservoir imaging using high-resolution traveltime tomography has proven successful at Hawaii (Okubo *et al.*, 1997), and volume estimates at mafic volcanoes such as Stromboli are possible using a comprehensive multi-disciplinary approach (Cigolini *et al.*, 2008). Geochemical tools such as U-series disequilibria provide another way of obtaining magma residence times and volumes beneath active volcanoes (Pyle, 1992; Gauthier & Condomines, 1999). Volume estimates of both resident and recharge magmas could provide an interesting tool to assess eruption style during future eruptive events.

Simultaneous effusion of lava during paroxysmal events is observed in some cases, and implies a secondary control by conduit dynamics. However, the fact that a minimum volume of recharge magma is required to produce an explosive event underlines the primary nature of the control exerted by reservoir dynamics.

Magma recharge appears to have opposite effects in mafic and silicic systems. Whereas more recharge means more explosive eruptions in mafic systems such as Volcán Llaima, observations of dacitic systems suggest that large volume fractions of recharge magma diminish the explosive character of the eruption (Mt Hood volcano, USA, Volcán Quizapu, Chile, Kent *et al.*, 2010; Ruprecht & Bachmann, 2010). This inverse relationship between how much recharge occurs and how explosive the resulting eruption can be, is due to the very different melt viscosities (~50 Pa s for Llaima and ~10^4–10^5 Pa s for Quizapu) and volatile contents (~2–3 wt % H_2O for Llaima and 4–6 wt % H_2O for Quizapu) of the erupted magmas. These differences are such that the magmas fragment according to different mechanisms.

In highly viscous magmas, the two commonly invoked mechanisms for fragmentation are (1) strain rates exceeding melt relaxation time (e.g. Papale, 1999) and (2) bubble overpressure exceeding magma strength (e.g. Zhang, 1998). In mafic magmas, however, neither of these processes is effective unless the magma is extensively cooled or crystallized. Instead, inertia of the magma generated by bubble expansion must be large enough for it to continue expanding and deforming until it fragments into discrete particles (Namiki & Manga, 2008). An increase in the volume fraction of recharge magma at Quizapu decreased the viscosity of the erupted magma through an increase in temperature and a change in composition, favoring efficient syn-eruptive degassing and reducing the potential for fragmentation (Ruprecht & Bachmann, 2010). An increase in the volume fraction of recharge magma at Llaima increases the inertial effects during magma ascent, which is the condition for fragmentation of a low-viscosity magma.

CONCLUSIONS

This study illuminates the hyper-active nature of Volcán Llaima through the observation of ubiquitous signs of magma mixing and mingling and a variety in styles of such interactions recorded by plagioclase phenocrysts. The study of texturally and compositionally distinct zones in the cores and rims of plagioclase phenocrysts yields a coherent picture of this complex, continuously evolving system, where shallow magma reservoirs contain highly viscous, crystal-rich magmas, the similar average compositions and partially molten states of which are maintained through frequent injections of low-viscosity, nearly aphyric, volatile-rich recharge magmas.

The comparison of tephra and lava pairs from two summit eruptions (AD 2008 and 1957) and a flank fissure eruption (Fissural 3, ~ AD 1850) at Volcán Llaima appears to manifest a common parent magma origin for Strombolian paroxysms and lava effusion. However, small but quantifiable differences in plagioclase and olivine zoning profiles and textures, as well as differences in phenocryst contents, with ~15–20 vol. % more phenocrysts in lavas than in tephra, indicate that a greater volume fraction of recharge magma was present in the explosively erupted magma than in the effusively erupted magma. We infer from these observations that Strombolian explosions at Volcán Llaima are favored by the injection of a large volume of recharge magma, which decreases the bulk viscosity and increases the volatile content of the erupted magma, favoring the large expansion velocities required for the fragmentation of low-viscosity magmas (basaltic-andesite in the Llaima case).

The observation of explosive eruptions generated by larger volume fractions of recharge magma in mafic systems is opposite to the observed behavior in silicic, volatile-rich volcanoes (Mt Hood and Volcan Quizapu; Kent *et al.*, 2010; Ruprecht & Bachmann, 2010), where more magma recharge means less explosive eruptions. Besides the fact that this apparent paradox is mostly due to the different melt viscosities, it stresses that in both mafic and silicic systems, conduit processes might not directly be responsible for the eruption style, but rather a consequence of the deeper pre-eruptive dynamics. Eruption style appears to be predetermined in the reservoir, where the dynamics of mixing between resident magmas and recharge magmas will define the crystal and volatile contents of the erupted magma.

ACKNOWLEDGEMENTS

We thank Jose-Antonio Naranjo, Hugo Moreno, Daniel Selles and the SENAGEOMIN for their help in the field and for providing access to the volcano during the period of eruptive activity in 2008. We were assisted in the field by Jason Jweda, Steve Goldstein, Pablo Salas and Olivier Reubi. We thank François Bussy for providing access to the EMPA laboratory, and Robert Bodner and Roel Verberne for their help during analysis. C.B.M. also would like to thank C. Ginibre for fruitful scientific conversations and useful advice from which this study greatly benefited. G. Wörner is thanked for the editorial handling of the paper, which was significantly improved in response to constructive reviews by Michael Carroll and two anonymous reviewers.

FUNDING

This project was supported by the Swiss NSF grant #20.125019 to M.A.D.

SUPPLEMENTARY DATA

Supplementary data for this paper are available at *Journal of Petrology* online.

REFERENCES

Aigner-Torres, M., Blundy, J., Ulmer, P. & Pettke, T. (2007). Laser ablation ICPMS study of trace element partitioning between plagioclase and basaltic melts: an experimental approach. *Contributions to Mineralogy and Petrology* **153**, 647–667.

Albarède, F. & Bottinga, Y. (1972). Kinetic disequilibrium in trace element partitioning between phenocrysts and host lava. *Geochimica et Cosmochimica Acta* **36**, 141–156.

Alidibirov, M. A. (1994). A model for viscous magma fragmentation during volcanic blasts. *Bulletin of Volcanology* **56**, 459–465.

Andrews, B. J., Gardner, J. E. & Housh, T. B. (2008). Repeated recharge, assimilation, and hybridization in magmas erupted from El Chichon as recorded by plagioclase and amphibole phenocrysts. *Journal of Volcanology and Geothermal Research* **175**, 415–426.

Asimow, P. D. & Ghiorso, M. S. (1998). Algorithmic modifications extending MELTS to calculate subsolidus phase relations. *American Mineralogist* **83**, 1127–1132.

Bacon, C. R. & Lowenstern, J. B. (2005). Late Pleistocene granodiorite source for recycled zircon and phenocrysts in rhyodacite lava at Crater Lake, Oregon. *Earth and Planetary Science Letters* **233**, 277–293.

Bai, C. Y. & Greenhalgh, S. (2005). 3D multi-step travel time tomography: Imaging the local, deep velocity structure of Rabaul volcano, Papua New Guinea. *Physics of the Earth and Planetary Interiors* **151**, 259–275.

Bathke, H., Shirzaei, M. & Walter, T. R. (2011). Inflation and deflation at the steep-sided Llaima stratovolcano (Chile) detected by using InSAR. *Geophysical Research Letters* **38**, L10304.

Berlo, K., Blundy, J., Turner, S. & Hawkesworth, C. (2007). Textural and chemical variation in plagioclase phenocrysts from the 1980 eruptions of Mount St. Helens, USA. *Contributions to Mineralogy and Petrology* **154**, 291–308.

Bindeman, I. N., Davis, A. M. & Drake, M. J. (1998). Ion microprobe study of plagioclase–basalt partition experiments at natural concentration levels of trace elements. *Geochimica et Cosmochimica Acta* **62**, 1175–1193.

Blackburn, E. A., Wilson, L. & Sparks, R. S. J. (1976). Mechanisms and dynamics of strombolian activity. *Journal of the Geological Society, London* **132**, 429–440.

Blundy, J. & Cashman, K. (2008). Petrologic reconstruction of magmatic system variables and processes. In: Putirka, K. D. & Tepley, F. J., III (eds) *Minerals, Inclusions and Volcanic Processes. Mineralogical Society of America and Geochemical Society, Reviews in Mineralogy and Geochemistry* **69**, *69179–239.*

Blundy, J. D. & Shimizu, N. (1991). Trace-element evidence for plagioclase recycling in calc-alkaline magmas. *Earth and Planetary Science Letters* **102**, 178–197.

Bouvet de Maisonneuve, C., Dungan, M. A., Bachmann, O. & Burgisser, A. (2012). Insights into shallow magma storage and crystallization at Volcan Llaima (Andean Southern Volcanic Zone, Chile). *Journal of Volcanology and Geothermal Research* **211**, 76–91.

Brophy, J. G., Dorais, M. J., Donnelly-Nolan, J. & Singer, B. S. (1996). Plagioclase zonation styles in hornblende gabbro inclusions from Little Glass Mountain, Medicine Lake Volcano, California: Implications for fractionation mechanisms and the formation of composition gaps. *Contributions to Mineralogy and Petrology* **126**, 121–136.

Browne, B. L., Eichelberger, J. C., Patino, L. C., Vogel, T. A., Uto, K. & Hoshizumi, H. (2006). Magma mingling as indicated by texture and Sr/Ba ratios of plagioclase phenocrysts from Unzen volcano, SW Japan. *Journal of Volcanology and Geothermal Research* **154**, 103–116.

Cashman, K. (2004). Volatile controls on magma ascent and eruption. In: Sparks, R. S. J. & Hawkesworth, C. (eds) *The State of the Planet: Frontiers and Challenges in Geophysics.* American Geophysical Union Monograph 150, pp. 109–124.

Chadwick, W. W., Jonsson, S., Geist, D. J., Poland, M., Johnson, D. J., Batt, S., Harpp, K. S. & Ruiz, A. (2011). The May 2005 eruption of Fernandina volcano, Galapagos: The first circumferential dike intrusion observed by GPS and InSAR. *Bulletin of Volcanology* **73**, 679–697.

Charlier, B. L. A., Wilson, C. J. N., Lowenstern, J. B., Blake, S., Van Calsteren, P. W. & Davidson, J. P. (2005). Magma generation at a large, hyperactive silicic volcano (Taupo, New Zealand) revealed by U–Th and U–Pb systematics in zircons. *Journal of Petrology* **46**, 3–32.

Cigolini, C., Laiolo, M. & Bertolino, S. (2008). Probing Stromboli volcano from the mantle to paroxysmal eruptions. In: Annen, C. & Zellmer, G. F. (eds) *Dynamics of Crustal Magma Transfer, Storage and Differentiation, Vol. 304.* Geological Society, London, Special Publications, pp. 33–70.

Couch, S., Harford, C. L., Sparks, R. S. J. & Carroll, M. R. (2003*a*). Experimental constraints on the conditions of formation of highly calcic plagioclase microlites at the Soufrière Hills Volcano, Montserrat. *Journal of Petrology* **44**, 1455–1475.

Couch, S., Sparks, R. S. J. & Carroll, M. R. (2003*b*). The kinetics of degassing-induced crystallization at Soufrière Hills volcano, Montserrat. *Journal of Petrology* **44**, 1477–1502.

Dingwell, D. B. (1996). Volcanic dilemma: Flow or blow? *Science* **273**, 1054–1055.

Dungan, M., Reubi, O., Bouvet de Maisonneuve, C., Bourdon, B., Langmuir, C., Bachmann, O. & Burgisser, A. (2009). Linking eruptive dynamics and frequency to petrologic and geochemical constraints at a hyperactive Andean arc volcano. *American Geophysical Union, Fall Meeting* , #V21C-1998.

Dzierma, Y. & Wehrmann, H. (2010). Eruption time series statistically examined: Probabilities of future eruptions at Villarrica and Llaima Volcanoes, Southern Volcanic Zone, Chile. *Journal of Volcanology and Geothermal Research* **193**, 82–92.

Finlayson, D. M., Gudmundsson, O., Itikarai, I., Nishimura, Y. & Shimamura, H. (2003). Rabaul volcano, Papua New Guinea: seismic tomographic imaging of an active caldera. *Journal of Volcanology and Geothermal Research* **124**, 153–171.

Gaetani, G. A., Ghiorso, M. S., Sack, R. O., Hirschmann, M. & Asimow, P. D. (1998). Melts. *Science* **282**, 1834–1835.

Gagnevin, D., Waight, T. E., Daly, J. S., Poli, G. & Conticelli, S. (2007). Insights into magmatic evolution and recharge history in Capraia Volcano (Italy) from chemical and isotopic zoning in plagioclase phenocrysts. *Journal of Volcanology and Geothermal Research* **168**, 28–54.

Gauthier, P.-J. & Condomines, M. (1999). ^{210}Pb–^{226}Ra radioactive disequilibria in recent lavas and radon degassing: inferences on the magma chamber dynamics at Stromboli and Merapi volcanoes. *Earth and Planetary Science Letters* **172**, 111–126.

Geist, D., Chadwick, W. & Johnson, D. (2006). Results from new GPS and gravity monitoring networks at Fernandina and Sierra Negra Volcanoes, Galapagos, 2000–2002. *Journal of Volcanology and Geothermal Research* **150**, 79–97.

Ghiorso, M. S. & Sack, R. O. (1995). Chemical mass transfer in magmatic processes IV. A revised and internally consistent thermodynamic model for the interpolation and extrapolatizon of liquid–solid equilibria in magmatic systems at elevated temperatures and pressures. *Contributions to Mineralogy and Petrology* **119**, 197–212.

Ginibre, C. & Worner, G. (2007). Variable parent magmas and recharge regimes of the Parinacota magma system (N. Chile) revealed by Fe, Mg and Sr zoning in plagioclase. *Lithos* **98**, 118–140.

Ginibre, C., Worner, G. & Kronz, A. (2002). Minor- and trace-element zoning in plagioclase: implications for magma chamber processes at Parinacota volcano, northern Chile. *Contributions to Mineralogy and Petrology* **143**, 300–315.

Gioncada, A., Mazzuoli, R. & Milton, A. J. (2005). Magma mixing at Lipari (Aeolian Islands, Italy): Insights from textural and compositional features of phenocrysts. *Journal of Volcanology and Geothermal Research* **145**, 97–118.

Gonnermann, H. M. & Manga, M. (2003). Explosive volcanism may not be an inevitable consequence of magma fragmentation. *Nature* **426**, 432–435.

Gonnermann, H. M. & Manga, M. (2007). The fluid mechanics inside a volcano. *Annual Review of Fluid Mechanics* **39**, 321–356.

Green, D. N., Neuberg, J. & Cayol, V. (2006). Shear stress along the conduit wall as a plausible source of tilt at Soufrière Hills volcano, Montserrat. *Geophysical Research Letters* **33**, L10306.

Hammer, C. & Neuberg, J. W. (2009). On the dynamical behaviour of low-frequency earthquake swarms prior to a dome collapse of Soufrière Hills volcano, Montserrat. *Geophysical Research Letters* **36.**

Houghton, B. F., Wilson, C. J. N., Del Carlo, P., Coltelli, M., Sable, J. E. & Carey, R. (2004). The influence of conduit processes on changes in style of basaltic Plinian eruptions: Tarawera 1886 and Etna 122 BC. *Journal of Volcanology and Geothermal Research* **137**, 1–14.

Housh, T. B. & Luhr, J. F. (1991). Plagioclase–melt equilibria in hydrous systems. *American Mineralogist* **76**, 477–492.

Humphreys, M. C. S., Blundy, J. D. & Sparks, R. S. J. (2006). Magma evolution and open-system processes at Shiveluch Volcano: Insights from phenocryst zoning. *Journal of Petrology* **47**, 2303–2334.

Jaupart, C. & Vergniolle, S. (1988). Laboratory models of Hawaiian and Strombolian eruptions. *Nature* **331**, 58–60.

Jentzsch, G., Punongbayan, R. S., Schreiber, U., Seeber, G., Volksen, C. & Weise, A. (2001). Mayon volcano, Philippines: change of monitoring strategy after microgravity and GPS measurements from 1992 to 1996. *Journal of Volcanology and Geothermal Research* **109**, 219–234.

Kent, A. J. R., Darr, C., Koleszar, A. M., Salisbury, M. J. & Cooper, K. M. (2010). Preferential eruption of andesitic magmas through recharge filtering. *Nature Geoscience* **3**, 631–636.

Kuritani, T. (1998). Boundary layer crystallization in a basaltic magma chamber: Evidence from Rishiri Volcano, Northern Japan. *Journal of Petrology* **39**, 1619–1640.

Landi, P., Metrich, N., Bertagnini, A. & Rosi, M. (2004). Dynamics of magma mixing and degassing recorded in plagioclase at Stromboli (Aeolian Archipelago, Italy). *Contributions to Mineralogy and Petrology* **147**, 213–227.

Lautze, N. C. & Houghton, B. F. (2007). Linking variable explosion style and magma textures during 2002 at Stromboli volcano, Italy. *Bulletin of Volcanology* **69**, 445–460.

Lofgren, G. (1980). Experimental studies on the dynamic crystallization of silicate melts. In: Hargraves, R. B. (ed.) *Physics of Magmatic Processes*. Princeton, NJ: Princeton University Press, pp. 487–565.

Longhi, J., Walker, D. & Hays, J. (1976). Fe and Mg in plagioclase. *Proceedings of the 7th Lunar Science Conference. Geochimica et Cosmochimica Acta Supplement*, pp. 1281–1300.

Lowry, A. R., Hamburger, M. W., Meertens, C. M. & Ramos, E. G. (2001). GPS monitoring of crustal deformation at Taal Volcano, Philippines. *Journal of Volcanology and Geothermal Research* **105**, 35–47.

Marsh, B. D. (1988). Crystal size distribution (CSD) in rocks and the kinetics and dynamics of crystallization. 1. Theory. *Contributions to Mineralogy and Petrology* **99**, 277–291.

Mason, R. M., Starostin, A. B., Melnik, O. E. & Sparks, R. S. J. (2006). From Vulcanian explosions to sustained explosive eruptions: The role of diffusive mass transfer in conduit flow dynamics. *Journal of Volcanology and Geothermal Research* **153**, 148–165.

Mastin, L. G. (2002). Insights into volcanic conduit flow from an open-source numerical model. *Geochemistry, Geophysics, Geosystems* **3**, 1037.

McBirney, A. & Murase, T. (1970). Factors governing the formation of pyroclastic rocks. *Bulletin of Volcanology* **34**, 372–384.

Miller, J. S., Matzel, J. E. P., Miller, C. F., Burgess, S. D. & Miller, R. B. (2007). Zircon growth and recycling during the assembly of large, composite arc plutons. *Journal of Volcanology and Geothermal Research* **167**, 282–299.

Nakamura, M. & Shimakita, S. (1998). Dissolution origin and syn-entrapment compositional change of melt inclusion in plagioclase. *Earth and Planetary Science Letters* **161**, 119–133.

Namiki, A. & Manga, M. (2008). Transition between fragmentation and permeable outgassing of low viscosity magmas. *Journal of Volcanology and Geothermal Research* **169**, 48–60.

Naranjo, J. A. & Moreno, H. (2005). *Geología del volcán Llaima, Región de la Araucanía. Carta Geológica de Chile, Serie Geología Básica, No. 88.* Santiago: Servicio Nacional de Geología y Minería, 33 p.

Nelson, S. T. & Montana, A. (1992). Sieve-textured plagioclase in volcanic rocks produced by rapid decompression. *American Mineralogist* **77**, 1242–1249.

Neuberg, J. (2006). Multi-parameter monitoring and modelling of volcanic processes. In: Mader, M. H., Coles, G. S. & Connor, B. C. (eds) *Statistics in Volcanology*. London: Special publications of IAVCEI, 1, Geological Society, pp. 215–230.

Okubo, P. G., Benz, H. M. & Chouet, B. A. (1997). Imaging the crustal magma sources beneath Mauna Loa and Kilauea volcanoes, Hawaii. *Geology* **25**, 867–870.

Papale, P. (1999). Strain-induced magma fragmentation in explosive eruptions. *Nature* **397**, 425–428.

Parfitt, E. A. & Wilson, L. (1995). Explosive volcanic eruptions. 9. The transition between Hawaiian-style lava fountaining and Strombolian explosive activity. *Geophysical Journal International* **121**, 226–232.

Pioli, L., Azzopardi, B. J. & Cashman, K. V. (2009). Controls on the explosivity of scoria cone eruptions: Magma segregation at conduit junctions. *Journal of Volcanology and Geothermal Research* **186**, 407–415.

Polacci, M., Rosi, M., Landi, P., Di Muro, A. & Papale, P. (2005). Novel interpretation for shift between eruptive styles in some volcanoes. *EOS Transactions American Geophysical Union* **86**, 333–336.

Pyle, D. M. (1992). The volume and residence time of magma beneath active volcanoes determined by decay-series disequilibria methods. *Earth and Planetary Science Letters* **112**, 61–73.

Roduit, N. (2002). JMicroVision: Image analysis toolbox for measuring and quantifying components of high-definition images, Version 1.2.7. http://www.jmicrovision.com/.

Roman, D. C., Neuberg, J. & Luckett, R. R. (2006). Assessing the likelihood of volcanic eruption through analysis of volcanotectonic earthquake fault-plane solutions. *Earth and Planetary Science Letters* **248**, 244–252.

Ruprecht, P. & Bachmann, O. (2010). Pre-eruptive reheating during magma mixing at Quizapu volcano and the implications for the explosiveness of silicic arc volcanoes. *Geology* **38**, 919–922.

Ruprecht, P. & Worner, G. (2007). Variable regimes in magma systems documented in plagioclase zoning patterns: El Misti stratovolcano and Andahua monogenetic cones. *Journal of Volcanology and Geothermal Research* **165**, 142–162.

Scandone, R., Cashman, K. V. & Malone, S. D. (2007). Magma supply, magma ascent and the style of volcanic eruptions. *Earth and Planetary Science Letters* **253**, 513–529.

Singer, B. S., Dungan, M. A. & Layne, G. D. (1995). Textures and Sr, Ba, Mg, Fe, K, and Ti compositional profiles in volcanic plagioclase—clues to the dynamics of calc-alkaline magma chambers. *American Mineralogist* **80**, 776–798.

Sisson, T. W. & Grove, T. L. (1993). Experimental investigations of the role of H_2O in calc-alkaline differentiation and subduction zone magmatism. *Contributions to Mineralogy and Petrology* **113**, 143–166.

Smithsonian Institution. (2008). *Llaima. Bulletin of the Global Volcanism Network* **33**, *33*.

Sparks, R. S. J., Biggs, J. & Neuberg, J. W. (2012). Monitoring volcanoes. *Science* **335**, 1310–1311.

Streck, M. J. (2008). Mineral textures and zoning as evidence for open system processes. In: Putirka, K. D. & Tepley, F. J., III (eds) *Minerals, Inclusions and Volcanic Processes. Mineralogical Society of America and Geochemical Society, Reviews in Mineralogy and Geochemistry* **69**, *69595–622*.

Streck, M. J., Dungan, M. A., Malavassi, E., Reagan, M. K. & Bussy, F. (2002). The role of basalt replenishment in the generation of basaltic andesites of the ongoing activity at Arenal volcano, Costa Rica: evidence from clinopyroxene and spinel. *Bulletin of Volcanology* **64**, 316–327.

Streck, M. J., Dungan, M. A., Bussy, F. & Malavassi, E. (2005). Mineral inventory of continuously erupting basaltic andesites at Arenal volcano, Costa Rica: implications for interpreting monotonous, crystal-rich, mafic arc stratigraphies. *Journal of Volcanology and Geothermal Research* **140**, 133–155.

Sturton, S. & Neuberg, J. (2006). The effects of conduit length and acoustic velocity on conduit resonance: Implications for low-frequency events. *Journal of Volcanology and Geothermal Research* **151**, 319–339.

Sugawara, T. (2000). Thermodynamic analysis of Fe and Mg partitioning between plagioclase and silicate liquid. *Contributions to Mineralogy and Petrology* **138**, 101–113.

Sugawara, T. (2001). Ferric iron partitioning between plagioclase and silicate liquid: thermodynamics and petrological applications. *Contributions to Mineralogy and Petrology* **141**, 659–686.

Sumner, J. M. (1998). Formation of clastogenic lava flows during fissure eruption and scoria cone collapse: the 1986 eruption of Izu-Oshima Volcano, eastern Japan. *Bulletin of Volcanology* **60**, 195–212.

Tsuchiyama, A. (1985). Dissolution kinetics of plagioclase in the melt of the system diopside–albite–anorthite, and origin of dusty plagioclase in andesites. *Contributions to Mineralogy and Petrology* **89**, 1–16.

Villiger, S., Ulmer, P. & Muntener, O. (2007). Equilibrium and fractional crystallization experiments at 0·7 GPa; the effect of pressure on phase relations and liquid compositions of tholeiitic magmas. *Journal of Petrology* **48**, 159–184.

Woods, A. W. (1995). The dynamics of explosive volcanic eruptions. *Reviews of Geophysics* **33**, 495–530.

Woods, A. W. & Koyaguchi, T. (1994). Transitions between explosive and effusive eruptions of silicic magmas. *Nature* **370**, 641–644.

Zhang, Y. (1998). Experimental simulations of gas-driven eruptions: kinetics of bubble growth and effect of geometry. *Bulletin of Volcanology* **59**, 281–290.

APPENDIX

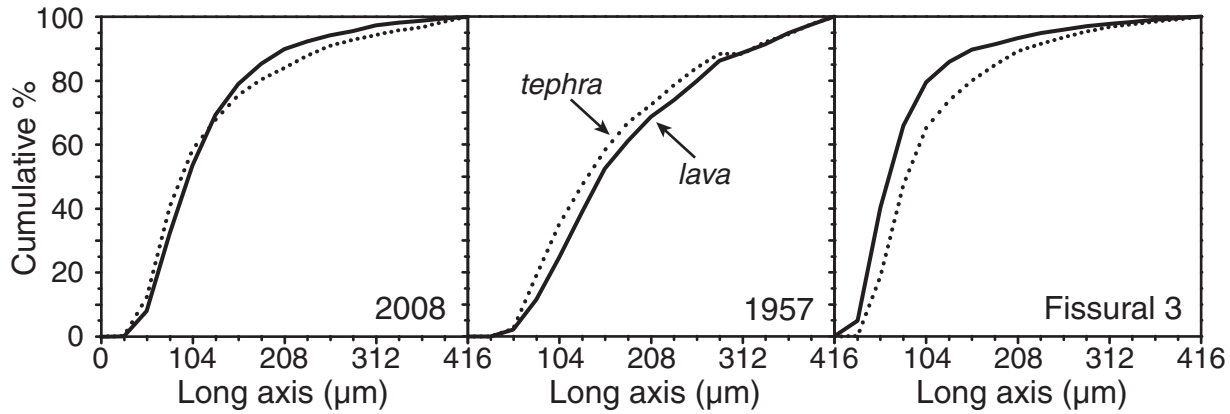

Fig. A1. Curves of the cumulative percentage of crystals within a given size range for the 2008, 1957, and Fissural 3 (~ AD 1850) eruptive events of Volcán Llaima. Measurement of the long axis of all the crystals present within a representative area of a thin section (~1·5 cm × 1·5 cm, 1000–2000 crystals per sample in the tephra, 2000–4000 crystals per sample in the lava) was performed using the image analysis software JMicroVision (Roduit, 2002). Overlap of the data for the tephra and lava produced during a same eruptive event suggests that lavas have not been severely modified by crystallization during eruption compared with the tephra. Phenocrysts thus record pre-eruptive reservoir conditions.